Comparative assessment of the effects of 3D printed feed spacers on process performance in MD systems

Comparative assessment of the effects of 3D printed feed spacers on process performance in MD systems

Navya Thomas[1], Jaichander Swaminathan[2], Guillermo Zaragoza[3], Rashid K. Abu Al-Rub[1], John H. Lienhard V[4], Hassan A. Arafat[1*]

[1] Center for Membranes and Advanced Water Technology, Khalifa University, Abu Dhabi, UAE
[2] Department of Mechanical Engineering, Indian Institute of Technology Gandhinagar, Gujarat, India
[3] CIEMAT-Plataforma Solar de Almería, Almería, Spain
[4] Rohsenow Kendall Heat Transfer Laboratory, Department of Mechanical Engineering, Massachusetts Institute of Technology, Cambridge, Massachusetts, USA

[*]corresponding author, Email: hassan.arafat@ku.ac.ae

Abstract

In this study, process enhancements achieved by the use of 3D printed feed spacers based on triply periodic minimal surfaces (TPMS) were comparatively assessed using the two most common membrane distillation (MD) configurations: air gap (AGMD) and direct contact (DCMD). The MD performance was assessed based on the impact of spacer design (TPMS vs. commercial spacer) on flux and feed channel pressure drop, and their consequent impact on the levelized cost of water (COW). The studied spacer architectures led to a minimal improvement (≤17%) in AGMD flux, much lower than that achieved in DCMD (≤57%). Consequently, for a waste heat-operated MD process, the spacer-induced channel pressure drop became the most influential cost bottleneck on COW. Generally, the contribution of the pumping cost to the total operating cost was found to be greater for DCMD than AGMD. Thus, the COW of a waste heat operated DCMD is more sensitive to a decrease in spacer-induced channel pressure drop than in an AGMD. For an MD process operated with additional heat cost, the flux improvement achieved using TPMS spacers reduces the thermal energy component of the operating cost. Ultimately, this predominantly contributes to a lower COW.

Keywords: Triply periodic minimal surfaces; feed spacers; membrane distillation; cost analysis; 3D printing

Nomenclature

Acronyms

ABS	acrylonitrile butadiene styrene
AGMD	air gap membrane distillation
CAPEX	capital expense
$CAPEX_{CS}$	capital cost of MD unit using commercial spacer, \$ per m^2 of membrane area
COW	cost of water, \$/m^3
COW_{CS}	cost of water using commercial spacer, \$/m^3
$COW_{CS\text{-}CAP}$	capital cost component of the cost of water using commercial spacer, \$/m^3
$COW_{CS\text{-}OP}$	operating cost component of the cost of water using commercial spacer, \$/m^3
$COW_{CS\text{-}OP\_pump}$	pumping energy cost component of the cost of water using commercial spacer, \$/m^3
$COW_{CS\text{-}OP\_th.energy}$	thermal energy cost component of the cost of water using commercial spacer, \$/m^3
$COW_{CS\text{-}OP\_rest}$	other operating costs component of the cost of water using commercial spacer, \$/m^3
COW_{TPMS}	cost of water using 3D printed TPMS spacer, \$/m^3
$COW_{TPMS\text{-}CAP}$	capital cost component of the cost of water using 3D printed TPMS spacer, \$/m^3
$COW_{TPMS\text{-}OP}$	operating cost component of the cost of water using 3D printed TPMS spacer, \$/m^3
CS	commercial spacer
DCMD	direct contact membrane distillation
DLP	digital light processing
FDM	fused deposition modeling
GOR	gained output ratio, dimensionless
LEP	liquid entry pressure, bar
MD	membrane distillation
OPEX	operating expense
PD_{CS}	pressure drop when using commercial spacer, bar
PD_{TPMS}	pressure drop when using commercial spacer, bar
PTFE	polytetrafluoroethylene
RC_{Flux}	relative change in flux when using the TPMS spacer

RC_{PD}	relative change in pressure drop when using the TPMS spacer
SGMD	sweep gas membrane distillation
SLA	stereolithography
SLS	selective laser sintering
TPMS	triply periodic minimal surfaces
VMD	vacuum membrane distillation

Romans

A	membrane area, m^2
d_{ch}	feed channel depth, m
d_h	feed channel hydraulic diameter, m
f	friction factor
h_{fg}	enthalpy of vaporization, J/kg
J_{CS}	permeate flux using commercial spacer, kg/m^2s
J_{TPMS}	permeate flux using 3D printed TPMS spacer, kg/m^2s
L	length of channel, m
$\dot{m}_f$	mass flow rate of feed, kg/s
$\dot{m}_p$	mass flow rate of product or permeate, kg/s
$\dot{Q}_{in}$	inlet heat transfer rate, W
v	flow velocity, m/s

Greek symbol

ρ	density

1 Introduction

In recent years, there has been a growing trend of studying the use of additive manufacturing (i.e., 3D printing) techniques to impart process and design enhancements in membrane systems [1]. The prime advantage of 3D printing over traditional manufacturing techniques is its ability to easily produce almost any complicated geometry across different scales by a layer-wise manufacturing process. 3D printing applications explored for membrane systems include membrane synthesis [2–6], spacer design [7–14] and fabrication of other membrane system components [15–17]. The majority of these studies have focused on spacer design, since the dimensional requirement of spacers is well aligned with the resolution range (0.1 to 10 μm) of current 3D printing technologies [18]. The application of 3D printing in creating various spacer designs has improved the membrane process performance by achieving increased flux [7–12], lower energy consumption [8,19], reduced fouling [7,10,11,13,20,21] and reduced channel pressure drop [13,22] with respect to the adoption of conventional spacers.

Membrane distillation (MD) technology has been heralded as an alternative separation technology for various applications, such as desalination, hypersaline brine management, wastewater treatment, textile and pharmaceutical residue treatment, etc. [23–25]. Traditionally, MD can be operated in four different configurations including direct contact MD (DCMD), air gap MD (AGMD), vacuum MD (VMD), and sweep gas MD (SGMD) [26]. However, AGMD has been the preferred MD configuration for pilot and demonstration plants, while DCMD is the preferred configuration for lab-scale performance assessment, as it is the simplest configuration to setup and operate [27]. In AGMD, the air gap reduces heat losses through conduction, resulting in improved thermal efficiency. However, compared to DCMD, the presence of the air gap also results in increased resistance to mass transfer, thus lower flux. Recent studies [28] have demonstrated the capability of vacuum enhanced AGMD operation to achieve higher flux and energy efficiency with AGMD, even while treating high salinity brine solutions.

A widely investigated strategy to enhance flux in MD modules is *via* feed channel spacers [29,30].

In addition to effecting inter-membrane spacing in flat-sheet membrane modules [31], including spiral wound elements, feed spacers function as turbulence promoters by inducing directional changes in the flow and generating significant secondary flow structures [32]. By inducing additional flow turbulence, feed channel spacers suppress the thermal and concentration boundary layers bordering the membrane, thus reducing the temperature and concentration polarization effects, enhancing flux, and minimizing foulant adhesion [33–35]. Nevertheless, the presence of spacer also increases the pressure drop over the feed channel [32]. In pressure-driven processes such as reverse osmosis, the pressure drop is a concern as it translates to higher pumping costs. However, in MD, a major concern with pressure drop is membrane wetting. The introduction of the spacers should restrict the hydraulic pressure drop, which has to be compensated for by increasing the incoming feed pressure, from exceeding the liquid entry pressure (LEP) of the membrane. If the hydraulic pressure of the entering feed exceeds the LEP, the hydrophobic membrane becomes unable to prevent the passage of liquid through its pores, leading to a degraded permeate quality.

Conventional feed spacers are mesh-like structures with filaments positioned bi-planarly in a woven or non-woven arrangement [36]. The characteristic geometric parameters of a mesh spacer include mesh length, filament thickness, hydrodynamic angle (angle between filaments), and flow attack angle (angle between filament and flow direction) (Fig. 1). Most reported studies on optimizing conventional mesh spacers have targeted these geometric parameters [37]. In the context of these parameters, creating an optimal mesh spacer could be limited, especially if the design requirements for achieving improved flux and reduced hydraulic pressure drop are in conflict. For instance, a recent study concluded that a spacer design with an increased number of thick filaments is theoretically recommended to maximize vapor flux while thinner and fewer filaments are recommended to minimize hydraulic pressure drop in DCMD [30]. The design capabilities of traditional manufacturing methods, such as molding and extrusion, limit innovations in mesh spacer geometries for enhanced process performance [38]. 3D printing, on the contrary, enables the creation of irregular, complex and intricate feed spacer geometries, which traditional manufacturing methods cannot easily achieve [1].

Despite the merits of 3D printing, such as design flexibility, the existing 3D printing technologies are impeded by the limitations of high cost, slow printing speed, poor scalability, restricted build size and limited resolution [1]. The cost of 3D printing is affected by the high capital cost of printers, material cost and the amount of resource material used. Consumer grade 3D printers with low resolution could be purchased for as low as $500, while industrial grade printers with high resolution and throughput can cost upwards of $1M [39]. Raw materials used can cost anywhere from $50/kg to $500/kg for resins, while exotic materials such as titanium can cost thousands of USD per ounce [40]. Another cost-related bottleneck of 3D printing is the deposition rate of material, which can be as low as 1/10,000 compared to conventional manufacturing methods [41]. As more researchers develop innovative 3D printed spacers, we aim to investigate in this work if the payoff from a 3D printed spacer, such as increased flux and energy efficiency and reduced pressure drop, can be justified within the context of 3D printing cost-ineffectiveness. For the analysis, we consider AGMD and DCMD as the use-case scenarios with triply periodic minimal surfaces (TPMS) [42] as the printed feed spacer design. We begin by comparing the effect of using TPMS spacer geometries on flux and pressure drop in AGMD and DCMD system and examine the reasons behind differences between the two configurations. We then conduct a cost analysis to assess whether 3D printed spacers can serve as a cost-effective alternative to conventional mesh spacers and under what conditions. To the best of authors' knowledge, this is the first article that focuses on comparing the performance of 3D printed spacers in the two most commonly applied MD configurations, using a holistic approach which considers the impacts of the new spacers on flux, pressure drop and the collective impact of these parameters on the final product water cost.

2 Methodology

For the comparative assessment, the performance of three different TPMS spacer geometries was compared in DCMD and AGMD configurations. The performance data of the TPMS spacers in a DCMD configuration were obtained from a previous study conducted by the authors [10]. The experimental data to assess the performance of TPMS spacer geometries in AGMD was obtained in this work as detailed below.

2.1 Materials

A flat sheet PTFE MD membrane (Memsys GmbH, Germany) was used in all experiments. The membrane properties as specified by the manufacturer are: nominal pore size: 0.2 µm, LEP: $\geq$ 3.5 bar, air permeability: 10-40 l/cm^2/h at 0.07 bar, and thickness: 160 $\pm$ 40 µm. Three TPMS architectures were investigated in this study for their performance in AGMD. These are: Schwarz P skeletal, Schoen Gyroid, and transverse Schwarz Crossed Layer of Parallels (CLP). These spacers will henceforth be referred to as P, Gyr and tCLP, respectively. Each of these TPMS topologies can be described in three-dimensional space by a level-set approximation equation [33, 36] as shown below, where the level-set parameter α represents the spacer voidage (i.e., porosity):

Schwarz P $\quad \cos x + \cos y + \cos z = \alpha \quad (1)$

Schoen Gyroid $\quad \sin x \cos y + \sin y \cos z + \sin z \cos y = \alpha \quad (2)$

Schwarz CLP $\quad \sin z \sin y - 0.4 \sin(1.2\, x) \cos z \cos y = \alpha \quad (3)$

The unit cell representations of these spacers along with the photographic images of the commercial mesh and 3D TPMS printed spacers are presented in Fig. 2. The geometrical characteristics of the TPMS spacers are presented in Table 1. In the tCLP design, there are channels aligned perpendicular to the feed flow direction as seen in Fig. 2. This design was conceived considering that such an arrangement would cause maximum flow disruption in the feed channel, creating greater turbulence. The TPMS spacers were 3D printed using the selective laser sintering (SLS) technique at a thickness of 4.0 mm and using polyamide (PA 2202, black, EOS) as the printing material. Details of the printing technique and its accuracy are discussed elsewhere [7,9]. The performance of the TPMS spacers in AGMD was benchmarked against a commercial mesh spacer (CS) (SWM, USA), which was made from high-density polyethylene with a 90° angle of intersection and a strand count of two per inch (≈ 78 strands per meter).

2.2 AGMD test setup

The evaluation of spacer performance was done using a laboratory-scale flat-sheet AGMD module (details listed in Table 2), operated in counter-current mode. The spacer to be tested was placed within the feed channel of the AGMD module. The air gap thickness was 1 mm and a plastic mesh spacer was used in all tests to keep the air gap thickness constant. The feed was heated using a resistance immersion heater with a feedback controller. The feed pipeline was equipped with sensors to monitor the flow rate, temperature and pressure drop across the membrane cell. The recirculating cold water stream (for condensation plate cooling) was maintained constant at 20 °C and was delivered from a cold reservoir tank. Detailed description of the AGMD setup can be found elsewhere [43]. The performance assessment of the spacers was done at three feed temperatures: 40, 50 and 65 °C generating driving forces equal to 51, 101 and 229 mbar, respectively. For each feed temperature, the flux was measured at four feed flow velocities: 0.07, 0.13, 0.21 and 0.30 m/s. The feed solution was a mixture of deionized and tap water with an average feed conductivity of 340 ± 25 µS/cm. Such feed was selected to allow the detection of membrane wetting.

2.3 Cost analysis

The impact of 3D printed spacers usage was assessed by evaluating its influence on water costs derived from MD. For more general validity, this analysis was performed in relative terms, that is, as a variation in the cost of water (COW) with and without the 3D printed spacers (ΔCOW, %). This approach allows others to build on our analysis by using their own COW components' values, which depend on the module design, configuration and performance, plant size and energy source [27]. The ΔCOW (%) was represented as:

$$\Delta COW\,(\%) = \left(\frac{COW_{TPMS} - COW_{CS}}{COW_{CS}}\right) \times 100\% \quad (4)$$

where COW_{TPMS} and COW_{CS} are the cost of water when using the 3D printed TPMS and commercial spacers, respectively. The COW is the sum of contributions from the capital and operating costs. Therefore, COW_{TPMS} and COW_{CS} can be represented as:

$$COW_{TPMS} = COW_{TPMS-CAP} + COW_{TPMS-OP} \quad (5)$$

$$COW_{CS} = COW_{CS-CAP} + COW_{CS-OP} \quad (6)$$

where $COW_{TPMS\text{-}CAP}$ and $COW_{CS\text{-}CAP}$ are the contributions of the capital cost to the respective COW values while $COW_{TPMS\text{-}OP}$ and $COW_{CS\text{-}OP}$ are the contributions of the operating costs to the COW, using the TPMS and CS, respectively. The cost analysis in this work was performed for both small (10 m^3/day) and large-scale (1000 m^3/day) MD plants, in order to account for the varying relative contribution of the capital and operating costs to the COW due to MD plant size. The first assumption made in this analysis was that the impact of the spacers on the capital cost component of the COW is due only to i) the added cost of the 3D printed spacers and ii) the change in flux, to which CAPEX is inversely proportional. Therefore, the capital cost component of the COW due to the use of 3D printed spacers can be calculated as per Eq. 7:

$$COW_{TPMS-CAP} = COW_{CS-CAP} \times \frac{(CAPEX_{CS} + 3D\ spacer\ cost)}{CAPEX_{CS} \times (1 + RC_{Flux})} \quad (7)$$

where $CAPEX_{CS}$ is the reference capital cost of the MD system in which a CS is used, normalized to membrane area and RC_{Flux} (dimensionless ratio) is the relative change in flux when using a TPMS spacer. Since both $CAPEX_{CS}$ and *3D spacer cost* are quantified in $USD per unit of membrane area, the second term on the right in Eq. 7 is dimensionless and is independent of the membrane area used in the module. It should be noted that the *3D spacer cost* was multiplied by two for the DCMD module, due to the spacers being used in both feed and permeate channels. In AGMD, the 3D printed spacer was considered to be only used in the feed channel, since the gap has its own commercial spacer. RC_{Flux} can be calculated as per Eq. 8:

$$RC_{Flux} = \frac{J_{TPMS} - J_{CS}}{J_{CS}} \quad (8)$$

where J_{TPMS} *and* J_{CS} are the permeate fluxes using the TPMS and CS spacers, respectively.

For each MD configuration and plant size, the analysis was based on two different $CAPEX_{CS}$ values: *current* and *prospective* (Tables 3 and 4). The current $CAPEX_{CS}$ costs for both small and large scale plants were based on the economic assessment of MD systems by Hitsov et al. [44]. On the other hand, the prospective values were determined assuming a potential 50% cost reduction in the CAPEX of MD system in the future, as a consequence of a wide-scale commercial implementation and manufacturing optimization of the MD technology. This assumption was based on correspondence with Aquastill B.V., a leading manufacturer of MD systems. The premise of using these values is that they can be applicable to all the spiral-wound MD modules. This premise is considered acceptable because similar materials are used in MD modules.

Another important factor in our CAPEX calculations is the cost of 3D printing (see Eq. 7), which is the most difficult to determine precisely because 3D printing is rapidly emerging and is very versatile in terms of printers, materials, economy-of-scale, etc. We found that there are several ranges for the cost of printing spacers, which could be extracted from i) research literature, ii) details provided by companies *via* private communication and iii) 3D printing platforms (e.g., Shapeways, iMaterialise, etc.). The cost of 3D printing is dependent on the type of printing technique, material cost and complexity of design. For example, in 2017, the reported material cost alone ranged from ~$200 to $300/kg for stereolithography (SLA), whereas the cost of material for fused deposition modeling (FDM) 3D printing ranged from ~$250 to $350/kg [4]. As per the latest 2020 report, the material cost for FDM filaments and SLA could be as low as $20/kg and ~$50/kg, respectively [39]. The material cost also varies depending on the scale of 3D printing. For a desktop 3D printer, the material cost can be as low as $19/kg and as high as $175/kg [4]. A recent study reported that the cost per part can be reduced by about 10% and 70-80% for SLS and FDM, respectively, by using material-reuse methods [45]. The study reported the cost of 3D printed parts using SLS as $225/kg for a single build based on a build-volume utilization of 15%, a build time of 12 h, a build temperature of 150 ºC, a cost for virgin powder of $50/kg and a cost for the grinding process of $13/kg. This cost would decrease to $201/kg if the material is reused until degraded beyond usefulness. Similarly, the cost of 3D printing was estimated to be \$173/kg for a single build with FDM with ABS material as support structures. This cost would drop to \$38/kg only if the material is used until it is degraded, that is, the reclaimed FDM materials from the build cycles are continuously milled, pelletized and reincorporated into the process using a filament extruder and winder [45]. The 3D printing cost assumed in this work is based on personal communication with a leading 3D printing company that uses the digital light processing (DLP) technique (company name is not disclosed here due to a confidentiality agreement). The cost of 3D printed spacers was assumed to be \$40 per m^2 of spacer area, using a high-throughput DLP technique and an average material cost of \$125/kg. This TPMS spacer cost was considered representative of commercial scale 3D printing cost with continuous production capacity. Please note that this cost is significantly lower than the cost declared by 3D printing platforms (such as Shapeways, iMaterialise, etc.) which operate based on discreet and small volume designs (e.g., printed by hobbyists, etc.). For comparison, the cost of a CS is only ~\$3/m^2 [46]. While the cost for 3D printed spacers considered in this work was determined to the best of our judgment, the methodology adopted here for cost analysis is sufficiently flexible for other researchers to extend this work by assuming different 3D printing costs.

With regards to $COW_{CS\text{-}OP}$, it was assumed that it is composed of three components: the COW components due to the pumping cost ($COW_{CS\text{-}OP\_pump}$), the COW components due to the thermal energy cost ($COW_{CS\text{-}OP\_th.energy}$), and the COW component due to the other operating costs which are unaffected by the type of spacer used (e.g., labor cost) ($COW_{CS\text{-}OP\_rest}$). The second main assumption made in this work is that switching to a TPMS spacer impacts the operating costs in two ways only: (i) by changing the cost of electrical energy based on the relative change in pressure drop, to which pumping energy is directly proportional, and (ii) by changing the thermal energy cost based on the relative change in flux. So, $COW_{CS\text{-}OP}$ and $COW_{TPMS\text{-}OP}$ were calculated as:

$$COW_{CS-OP} = COW_{CS-OP\_pump} + COW_{CS-OP-th.energy} + COW_{CS-OP\_rest} \tag{9}$$

$$COW_{TPMS-OP} = COW_{CS-OP\_pump}(1 + RC_{PD}) + \frac{COW_{CS-OP-th.energy}}{1 + RC_{flux}} + COW_{CS-OP\_rest} \quad (10)$$

$$RC_{PD} = \frac{PD_{TPMS} - PD_{CS}}{PD_{CS}} \quad (11)$$

where RC_{PD} is the relative change in pressure drop and PD_{TPMS} and PD_{CS} are the pressure drops when TPMS spacers and CS are used, respectively. Based on equations 4-7, 9 and 10, ΔCOW (%) can be represented as follows:

$$\Delta COW(\%) = \left(\frac{COW_{CS-CAP} \times \frac{(CAPEX_{CS} + 3D\ spacer\ cost)}{CAPEX_{CS} \times (1 + RC_{Flux})} + COW_{CS-OP_{pump}}(1 + RC_{PD}) + \frac{COW_{CS-OP-th.energy}}{1 + RC_{flux}} + COW_{CS-OP_{rest}}}{COW_{CS-CAP} + COW_{CS-OP}} - 1 \right) \times 100\% \quad (12)$$

The MD cost analysis by Hitsov et al. [44] was used to obtain $COW_{CS\text{-}CAP}$, $COW_{CS\text{-}OP}$, $COW_{CS\text{-}OP\_pump}$ and $COW_{CS\text{-}OP\_rest}$ (Tables 3 and 4). We considered two separate scenarios regarding $COW_{CS\text{-}OP\_th.energy}$: i) free (waste) heat, which is the basis for the cost calculations conducted in [44], and ii) \$5/m^3 for heat cost, which is reasonable for solar thermal energy powered MD [61]. Please note that the referenced model in [44] was based on membrane module lifetime of 5 years, a set depreciation period of 10 years and zero percent as the loan interest rate. When considering the prospective cost scenarios, only $COW_{CS\text{-}CAP}$ was reduced in the same proportion as $CAPEX_{CS}$ and $COW_{TPMS\text{-}CAP}$ was recalculated accordingly, but $COW_{CS\text{-}OP}$ were assumed not to change. Finally, for more general validity, ΔCOW was calculated for all the mentioned scenarios based on a hypothetical range of values for the relative change of flux (RC_{Flux}) and pressure drop (RC_{PD}) that could result from using a 3D printed spacer compared to those using a CS. By using Eq. 12 and the parameters presented in Tables 3 and 4, other researchers can easily perform a similar cost analysis to assess the cost effectiveness of any 3D printed spacer design in MD based on its flux and pressure drop performance and for any given 3D printing cost.

3 Results and Discussion

3.1 Effect of TPMS spacers on AGMD flux performance

A comparison of the AGMD flux performance using TPMS spacers, CS and no-spacer condition (i.e., empty feed channel) is presented in Fig. 3. As expected, an increase in feed temperature led to a considerable increase in permeate flux, since the saturation water vapor pressure on the feed side increases exponentially with feed temperature [47]. The rise in feed flow velocity was accompanied by a slight and asymptotic increase in flux, similar to previously reported data [48–52]. The introduction of spacers improved the AGMD flux relative to the empty channel. The most pronounced flux improvement was using the TPMS P spacer, under the combined operating conditions of highest feed temperature (65 ^{o}C) and lowest feed velocity (0.07 m/s), whereby the flux increased by 58% (Fig. 3a). The addition of a spacer interferes with the formation of thermal boundary layers near the membrane surface through increased mixing, thus reducing the effect of temperature polarization and increasing the flux. Compared to the CS, the TPMS P spacer increased the flux by up to 17% at a feed temperature of 65 ^{o}C. However, the impact of varying TPMS spacer geometry was not substantial. For example, at a feed temperature of 65 ^{o}C, the flux variation between the different TPMS spacer geometries ranged from 9 to 18%. This range is similar to previously reported improvement ranges of AGMD flux upon varying a mesh spacer design. An AGMD flux increase of only 4 to 10% was reported by varying the hydrodynamic angle from 60 to 120° for a carbon-fiber spacer, while reducing the filament thickness of the said spacer from 3 to 2 mm increased the flux by only 5% [53]. In an earlier study, the AGMD flux improved by 20 to 30% by varying mesh spacer design based on hydrodynamic angle, flow attack angle and filament shape [54]. Alternatively, the corrugation of AGMD feed channel has been reported to increase flux by 16-32% compared to the increase in flux (5-20%) by adding a mesh spacer [55].

More pronounced than its impact on flux, the choice of a spacer design had a significant impact on the channel pressure drop in AGMD. Fig. 4a displays the impact of varying the TPMS spacer geometry on channel pressure drop. The TPMS P and Gyr spacers reduced the pressure drop by 50% and 19%, respectively, relative to the CS. The tCLP spacer, on the other hand, resulted in nearly three-fold higher pressure drop than the CS. The channel pressure drop caused by the feed spacer is rooted in the resistance to flow exhibited by the spacer filaments (in the case of CS) or sheets (in the case of TPMS spacers), which in turn depends on the flow attack angle [56]. Indeed, the transverse arrangement of the channels in the tCLP design (which was deliberately chosen to cause maximum disruption to the approaching fluid flow and to create higher shear rates) caused the observed high pressure drop relative to the CS due to higher kinetic losses in the channel [57]. The abrupt change in flow direction by the transverse arrangement of spacer sheets imparts major pressure drag [58]. Furthermore, the tCLP design had the largest specific surface area of all TPMS spacers (7.9 mm^{-1}). This translates to more friction between the spacer sheets and the flow. In comparison, the P and Gyr spacers (with lower specific surface areas of 3.1 and 4.1 mm^{-1}, respectively) exhibited lower channel pressure drops. The overall impact of spacer geometry on MD performance can be gauged based on the spacer efficiency, defined as the ratio of flux produced by a given spacer at a given Reynolds number to the corresponding channel pressure drop [54]. The TPMS spacers P and Gyr, which resulted in lower channel pressure drop than the CS, exhibited relatively higher spacer efficiencies (Fig. 4b).

These results indicate that while the turbulence promoting TPMS spacer designs effect a limited flux enhancement in AGMD, the more likely benefit of an optimized TPMS spacer design in AGMD applications would be a reduced channel pressure drop. The reduced channel pressure drop achieved using TPMS spacer designs presents an opportunity to use AGMD modules with a longer feed channel, which in turn improves the efficiency of the internal heat recovery of the module.

3.2 Performance of TPMS spacers in AGMD vs. DCMD

An interesting finding from the evaluation of different spacers' performances in AGMD was that the variations in TPMS spacer topologies did not cause a significant increase in flux relative to the CS. As it initially appears, this is in contradiction with our earlier observed significant impact of TPMS spacers on flux in DCMD systems [10]. To illustrate this, Fig. 5 presents a comparison of the flux and pressure drop ratio of three different TPMS spacer geometries relative to a CS in both AGMD and DCMD configurations. The data for DCMD was obtained from an earlier work reported by the authors at 65 ^{o}C and 30 ^{o}C as feed and permeate temperatures, respectively [10]. Compared to the CS, the tCLP TPMS spacers increased the flux by up to 57% in DCMD. On the other hand, the highest flux improvement with a TPMS spacer in the AGMD system was only 17%. Upon considering the impact of spacer geometry on channel pressure drop, the Gyr and tCLP spacers caused a considerably higher pressure drop than the CS in DCMD. For instance, the tCLP spacer caused a 14-fold rise in pressure drop, compared to CS.

The mass and heat transfer resistances of the AGMD versus DCMD can explain the difference in TPMS spacer flux performance the two MD processes. Compared to DCMD, the presence of the air gap (ca. 1-2 mm thick) in AGMD increases the overall thermal resistance and helps reduce conductive heat losses. The resistances associated with vapor transport and heat conduction between the evaporation and condensation interfaces are often considered to be in parallel. The resistance associated with vapor transport is a function of the temperatures of the evaporation and condensation interfaces since saturation vapor pressure is an exponential function of temperature. A simple resistance network model accounting for the channels and transport across the membrane and air gap (Fig. 6) is herein adapted from Swaminathan et al. [59] to explain the observed difference in flux improvement in AGMD and DCMD upon using TPMS spacers.

In the case of an empty (spacer-less) feed channel (assuming channel heat transfer coefficients of 1000 W/m^{2}K, obtained by fitting the experimental data in [9]), the flux of DCMD is 75% higher than that of AGMD, owing to the additional resistance associated with the 1 mm thick air gap in AGMD. The boiling point elevation was assumed to be 1°C when evaluating the membrane resistance. In DCMD, the channels together account for 20 cm^{2}K/W out of the total resistance of 25.8 cm^{2}K/W. On the other hand, in AGMD, the total resistance is higher (48 cm^{2}K/W), with the major portion coming from the membrane and the air gap (28 cm^2K/W). When the channel heat transfer coefficients are increased by four-fold upon the use of TPMS spacers, as shown by Thomas et al. [9], the flux increases by 2.8 times in DCMD. Notice that the membrane resistance is also reduced with increasing temperature drop across the membrane. In contrast, in AGMD, the same increase in feed channel heat transfer coefficient results in a much smaller flux enhancement of about 25% (Fig. 6), which corresponds well with the experimental observations in the present study.

3.3 Energy benefits of using TPMS spacers in MD systems

The gained output ratio (GOR) of an MD system is defined as its inverse specific thermal energy consumption, non-dimensionalized by multiplying with the enthalpy of evaporation [60]:

$$GOR = \frac{\dot{m}_{\mathrm{p}} h_{\mathrm{fg}}}{\dot{Q}_{\mathrm{in}}} \tag{13}$$

It indicates how effectively the supplied heat input is recycled within the MD system to evaporate water from the feed 'more than once'. A small-scale MD system without energy recovery from the condensing vapor is limited to a GOR value lower than 1. However, pilot AGMD systems achieve significantly better energy efficiency by preheating the feed stream using the condensing vapor. The GOR of AGMD is proportional to the membrane area (*A*) [60]:

$$\mathrm{GOR} \propto \frac{A}{\dot{m}_{\mathrm{f}}} = \frac{1}{\rho d_{\mathrm{ch}}} \frac{L}{v} \tag{14}$$

In the above expression, d_{ch} is the feed channel depth, L is the channel length and v is the flow velocity. One can observe that GOR is proportional to the residence time of the feed within the MD module $\left(\frac{L}{v}\right)$. A recent study reported data from two pilot-scale AGMD modules of different sizes [28]. The larger module, which had a 3.6 times higher residence time, achieved 3 to 3.3 times higher GOR under identical operation conditions (top temperature and feed flow rate). This demonstrates the critical impact of the module length on system energy efficiency.

Pressure drop restrictions impose an upper limit on the value of residence time that can be achieved in an MD system. At a given feed velocity, chosen in order to achieve sufficiently high channel heat transfer coefficient, the overall pressure drop can be expressed in terms of the friction factor (f) and channel hydraulic diameter (d_{h}) as:

$$\Delta P = \frac{fL}{d_{\mathrm{h}}}\left(\frac{1}{2}\rho v^2\right) \tag{15}$$

The requirement that ΔP must be lower than the liquid entry pressure limits the maximum membrane/feed channel length that can be used. So, if a TPMS spacer has a significantly lower friction factor (f), observed in terms of a lower pressure drop than a CS at the same feed velocity and channel length, it enables the feed channel length to be increased by the same factor and would result in a corresponding improvement in GOR. Therefore, a 50% reduction in AGMD pressure drop compared to a CS, as observed in this study, presents an opportunity to increase the process GOR by nearly 2 times, *via* designing the feed channel to be 2X longer. In order to accurately estimate the improvement in GOR that can be achieved with these TPMS spacers, their pressure drop has to be experimentally determined with channel geometry and feed flowrate that correspond to those used in pilot-scale spiral wound MD systems.

Note that the longer module length discussed above results in an improvement in energy efficiency while producing the same total amount of pure water, at a reduced flux. This would be desirable if the cost of thermal energy is significant relative to the cost of system area. If, however, the opposite is true, then it is desirable to operate at higher flux even at the expense of lower energy efficiency. In such a case, a low value of L/v is preferred to achieve a larger driving temperature difference and hence flux. With a TPMS spacer that reduces friction factor by 50% using the same channel length, the velocity can be increased by 1.22 times while maintaining the same pressure drop. Correspondingly, the L/v ratio is decreased by around 18%, which helps increase the operating flux. If pumping electrical energy consumption is a more significant cost component than thermal energy, both L and v can be maintained the same, in order to reduce the pumping energy demand by around 50% by using the TPMS spacer, along with minor improvements in energy efficiency and flux.

In the above discussion, we have considered channel length to be limited by pressure drop. However, in practice, especially when MD is used for desalination of high salinity streams, a maximum allowable channel length can also be dictated by the need to maintain temperature drop across the membrane sufficiently higher than the feed boiling point elevation (BPE, which is proportional to salinity). If the transmembrane temperature drop falls close to BPE, a significant portion of energy transport across the membrane is through heat conduction, resulting in lower pure water production. In such cases, feed spacers that help reduce the channel concentration and temperature polarization without increase in pressure drop are particularly useful to increase temperature drop across the membrane and decrease BPE at the membrane interface.

3.4 Cost implications of using 3D printed spacers in AGMD vs. DCMD

The economic impact of using 3D printed spacers on the COW was assessed by estimating the relative change in COW, as described in Section 2.3. The variation in COW (ΔCOW, %), was calculated as a function of the relative changes in both flux (RC_{flux}) and pressure drop (RC_{PD}) due to using a 3D printed spacer instead of a CS. Figs. 7 and 8 show ΔCOW depictions for small-scale (10 m^3/day) DCMD and AGMD systems, respectively. The 3D plots were generated for two values of the MD reference capital costs; current and prospective, and two scenarios for thermal energy cost; free (waste) heat and additional heat cost, as detailed in Section 2.3. The sub-plots are labeled in the format xxx-y, wherein 'xxx' indicates the MD reference capital cost and 'y' indicates the presence or absence of heat cost. The green region in these plots indicates a favorable negative ΔCOW (i.e., a reduction in COW), while the red region reflects an unfavorable increase in COW. Additionally, based on the previously determined RC_{flux} and RC_{PD} values for TPMS spacers (see Sections 3.1 and 3.2), the ΔCOW values for these spacers were calculated and are also shown on Figs. 7 and 8.

For a small-scale DCMD plant (Fig. 7), the use of all the three TPMS spacers caused an unfavorable increase in COW compared to CS for all the different cost scenarios except for the combination of current $CAPEX_{CS}$ with additional heat cost, where only the Gyr spacer yielded a slightly favorable cost performance. The Gyr spacer, characterized by an RC_{flux} of +16.5% and an RC_{PD} of +94.4%, reduced the COW by merely 1.1% (Table 5). The TPMS spacers tCLP and Gyr-tCLP contributed to a rise in COW, despite resulting in a considerable RC_{flux} of +56.7%. The positive ΔCOW values in this case are caused by the considerable increase in pressure drop when using these spacers (1336% and 489%, respectively). For the cost scenarios with waste heat, the increase in COW for DCMD was predominantly dictated by the hydraulic resistance exerted by the TPMS spacers, regardless of the positive RC_{flux} these spacers yielded. This is because the increase in channel pressure drop was about one order of magnitude greater than the increases in flux with these TPMS spacers. Therefore, due to additional pumping requirements, the higher operating costs dwarfed any other cost savings effected by increased permeate productivity. On the contrary, for the cost scenarios with additional heat cost, it can be observed that for a given TPMS spacer the ΔCOW (%) is lower than the corresponding ΔCOW (%) with waste heat. This is because the relative flux improvement achieved by using a TPMS spacer reduces the additional thermal energy cost by a similar ratio, thus decreasing the operating cost component of the COW compared to the CS.

The premise is different for a small-scale AGMD plant compared to a DCMD plant. The economic impact of 3D printed spacers on the system CAPEX is halved as they are only used in one channel in AGMD, instead of two channels in DCMD. Among the three 3D printed TPMS spacers, the P spacer consistently exhibited a favorable drop in COW for all the four different scenarios considered for the small-scale AGMD plant (Table 6 and Fig. 8). The COW using the P spacer dropped by 5.1 and 1.7% for the current and prospective $CAPEX_{CS}$ with waste heat, respectively. The COW using the P spacer dropped further to 9.2 and 8.2% for the current and prospective $CAPEX_{CS}$ with additional heat cost, respectively. The performance of the P spacer in AGMD was characterized by only a moderate flux improvement of 17.4%, accompanied by a considerable (49.5%) decrease in pressure drop over the CS.

For large-scale (1000 m^3/day) production capacity, the economies of scale reduce the $CAPEX_{CS}$.

For instance, the current $CAPEX_{CS}$ drop by 77.3% and 75.7% for DCMD and AGMD, respectively, when the plant production capacity increases to 1000 m^3/day. At large-scale plant capacity, for DCMD (Fig. 9), all the TPMS spacers contribute to an increase in COW. As explained previously, this is attributed to the considerable increase in pressure drop despite the achieved improvement in flux. For the best-case spacer, Gyr for DCMD, the minimum increase in COW was 0.7% and 1.5%, corresponding to the current and prospective MD cost with additional heat cost. For a large-scale AGMD plant (Fig. 10), the COW increased with all TPMS spacers for the current and prospective $CAPEX_{CS}$ with waste heat. The COW using only the P spacer dropped by -9.2% and -8.9% for the current and prospective $CAPEX_{CS}$, respectively, with additional heat cost. While the economies of scale decreased the specific costs of MD systems, the cost of printing the TPMS spacers remained unchanged and, hence, the contribution of the TPMS spacers cost to the CAPEX of large-scale MD systems became more prominent.

For a better understanding of the observed impacts of printed spacers on COW, a breakdown of cost elements in the baseline scenarios using CS are herein discussed. The COW breakdown for small and large-scale AGMD and DCMD plants, based on current $CAPEX_{CS}$ and using CS spacers, is presented in Fig. 11 for the two scenarios: using waste heat and additional heat cost. For the small-scale production capacity with waste heat, $COW_{CS\text{-}OP}$ contributes 48% of the COW for DCMD and AGMD. The contribution of $COW_{CS\text{-}OP}$ to the COW increases to 66 and 70% for DCMD and AGMD, respectively, with additional heat cost. The contribution of $COW_{CS\text{-}OP\_pump}$ to $COW_{CS\text{-}OP}$ is generally greater in the DCMD configuration than in AGMD. When operating with waste heat, the $COW_{CS\text{-}OP\_pump}$ accounts for 25% and 8.3% of $COW_{CS\text{-}OP}$ for DCMD and AGMD, respectively. However, when additional heat cost is considered, the contribution of $COW_{CS\text{-}OP\_pump}$ diminishes to 11.7 and 3.3% of $COW_{CS\text{-}OP}$ for DCMD and AGMD, respectively, while $COW_{CS\text{-}OP\_th.energy}$ becomes a major component of $COW_{CS\text{-}OP}$. In the scenario with additional heat cost, $COW_{CS\text{-}OP\_th.energy}$ contributes to 53.2% and 60.2% of $COW_{CS\text{-}OP}$ for DCMD and AGMD, respectively. For the large-scale production capacity, $COW_{CS\text{-}OP}$ contributes to more than 70% of the COW with waste heat for both DCMD and AGMD configurations. With the additional heat cost, the contribution of $COW_{CS\text{-}OP}$ to the COW further increases to nearly 90% for both configurations but the percentage attributed to the $COW_{CS\text{-}OP\_pump}$ decreases. For instance, the additional heat cost decreases the contribution of the $COW_{CS\text{-}OP\_pump}$ to $COW_{CS\text{-}OP}$ from 35.4% to 11.2% for 1000 m^3/day DCMD and from 12.7 to 3.1% for 1000 m^3/day AGMD. The $COW_{CS\text{-}OP\_th.energy}$ contributes 68.5% and 75.2% of $COW_{CS\text{-}OP}$ of a large-scale DCMD and AGMD, respectively with additional heat cost. This cost breakdown indicates that when operating an MD plant with waste heat, the COW will be reduced by a 3D printed spacer design that predominantly achieves a decrease in the channel pressure drop compared to a CS and thus reduces the $COW_{CS\text{-}OP}$. Given the understanding that the contribution of the $COW_{CS\text{-}OP\_pump}$ to $COW_{CS\text{-}OP}$ is generally greater in DCMD than AGMD, the decrease in COW caused by the reduction in channel pressure drop will be more pronounced for the DCMD configuration. On the other hand, when operating an MD plant with additional heat cost, the flux increase achieved by a 3D printed spacer will impact the COW by decreasing the $COW_{CS\text{-}OP\_th.energy}$ which is a major component of $COW_{CS\text{-}OP}$ in this case.

To illustrate this further, one can assess the results gathered from a simple cost sensitivity analysis performed based on variations in flux and pressure drop (information pertaining to all the use-cases considered in the cost sensitivity analysis is tabulated in electronic Supplementary Information, SI). In the cost sensitivity analysis, ΔCOW was calculated for RC_{Flux} ranging from -10% to 100% and RC_{PD} ranging from -100% to 10% at 10% increment intervals. For a small-scale MD plant operated with waste heat, by using a 3D printed spacer design that exhibits no relative change in pressure drop compared to a CS (i.e. RC_{PD} equals zero), a drop in COW will begin to emerge with RC_{Flux} as little as 10 and 20% in DCMD (ΔCOW = -2.3%) and AGMD (ΔCOW = -3.8%), respectively. For a small-scale MD plant operated with additional heat cost, by using a 3D printed spacer design such that RC_{PD} equals zero, ΔCOW equals -4.7% and -3.5% with just 10% RC_{Flux} in DCMD and AGMD configurations, respectively. By using a 3D printed spacer design that exhibits no relative change in flux compared to a CS (i.e. RC_{Flux} equals zero) in a small-scale MD plant operated with waste heat, a reduction in COW will only begin to emerge at RC_{PD} of -30% in DCMD (ΔCOW = -1.0%), while for AGMD the COW will increase by 1.1% even if the pressure drop was reduced by -100%. This highlights that the COW of a DCMD plant operated with waste heat is more sensitive to a reduction in channel pressure drop than an AGMD plant. For a large-scale DCMD plant, by using a 3D printed spacer design such that RC_{PD} equals zero, a drop in COW will begin to emerge with RC_{Flux} equal 30% and 10% flux with waste heat (ΔCOW = -1.7%) and additional heat cost (ΔCOW = -4.3%), respectively. In other words, when operating a large-scale DCMD plant with additional heat cost, the use of a 3D printed spacer design that induces the same channel pressure drop as a commercial spacer but improves the flux by only 10% leads to cost savings. For a 1000 m^3/day AGMD plant, by using a 3D printed spacer design such that RC_{PD} equals zero, a drop in COW will begin to emerge with RC_{Flux} of 50% and 10% with waste heat (ΔCOW = -1.6%) and additional heat cost (ΔCOW = -3.0%), respectively. This observation highlights the significance of the improvement in flux achieved by the use of a 3D printed spacer for a large-scale MD plant operated with additional heat cost.

Another sensitivity analysis was conducted by considering the cost of printed spacers. Since 3D printing is a rapidly developing manufacturing technology, the future of 3D printing is believed to bring about reduced cost of 3D printing equipment and materials. Considering this, the last scenario we considered for the cost sensitivity analysis assumes the cost of 3D printed spacer to be halved to \$20/m^2. The impact of the reduced cost for 3D printed spacers was assessed for the future prospective $CAPEX_{CS}$ for both small and large-scale DCMD and AGMD plants operated with waste heat and additional heat cost (Figs. 12 and 13). For both small- and large-scale MD plants, the reduction in the cost of 3D printed spacer caused a greater drop in COW for the cost scenarios with waste heat as compared to the cost scenarios with additional heat cost. For instance, with the selected TPMS spacers in a small-scale AGMD plant, the decrease in the cost of 3D printed spacer further reduces the COW by ~4% on average for the scenario with waste heat and by only ~2% for the scenario with additional heat cost. Similarly, for a large-scale AGMD plant the decrease in the cost of 3D printed spacer further reduces the COW by ~8% on average for the scenario with waste heat and by only ~2% for the cost scenario with additional heat cost. Thus, the reduction in the cost of 3D printed spacers by 50% does not translate to substantial drop in the COW for the different scenarios.

4 Conclusions

This study has shown that the turbulence promoting TPMS spacer designs lead to limited flux enhancement in AGMD. The more likely benefit of an optimized TPMS spacer design for AGMD would be a reduced channel pressure drop with respect to the adoption of convetionally used commercial mesh spacers. The use of different TPMS spacer geometries in AGMD presented only a marginal flux improvement (up to 17%) compared to commercial mesh spacer. The observed flux improvement in AGMD with TPMS spacer was considerably low compared to the flux improvement (up to 57%) obtained in a DCMD configuration. This is attributed to the increased mass transfer resistance imposed by the air gap in AGMD configuration, thereby limiting the spacer-induced improvement in flux that accompanies better heat transfer within the feed channel. Despite the limited flux improvement, the choice of TPMS spacer geometry in AGMD had rather pronounced effect on channel pressure drop affirmed by the 50% lower pressure drop obtained by the P spacer compared to a commercial spacer. This reduced channel pressure drop presents the opportunity to design AGMD modules with double the membrane length and can thus increase the GOR by nearly two times. The cost implications of using the selected 3D printed TPMS spacers in a small and large-scale DCMD and AGMD module was also assessed in the study based on the relative change in cost of water (*ΔCOW*) contributed by the change in flux and pressure drop over a commercial spacer. The cost analysis considered two separate scenarios for thermal energy cost – waste heat and additional heat cost of $5/m^3. Since the channel pressure drop is directly proportional to the electrical energy associated with the pumping cost, it influences the operating cost component (OPEX) of the COW. Thus, for an MD plant operated with waste heat, the 3D printed spacer-induced channel pressure drop becomes the bottleneck in influencing the COW. The contribution of the pumping cost to the total operating cost is generally greater for the DCMD configuration than AGMD. Thus, the COW of a DCMD plant operated with waste heat is more sensitive to a reduction in spacer-induced channel pressure drop than an AGMD plant. In scenarios wherein the MD plant is operated with additional heat cost, flux improvement achieved by using a 3D printed spacer reduces the thermal energy component of the operating cost, predominantly contributing to reduced COW. The cost analysis reveals that a cost-effective 3D printed spacer design should achieve flux improvement without additional penalties on channel pressure drop while the best-case scenario would be a 3D printed spacer design that improves the flux throughput while simultaneously reducing the channel pressure drop relative to the commercial mesh spacer design.

Acknowledgment

The TPMS spacers were printed using Core Technology Platform resources at NYU Abu Dhabi. We thank Dr. Reza Rowshan, Dr. Oraib Al-Ketan and Khulood Alawadi (NYU Abu Dhabi) for their support and assistance with 3D printing. We thank Nurshaun Sreedhar for useful discussions and feedback on the manuscript. The authors from the Center for Membrane and Advanced Water Technology acknowledge that this publication is based upon work supported by the Khalifa University of Science and Technology under Award No. RC2-2018-009.

References

[1] L.D. Tijing, J.R.C. Dizon, I. Ibrahim, A.R.N. Nisay, H.K. Shon, R.C. Advincula, 3D printing for membrane separation, desalination and water treatment, Appl. Mater. Today. 18 (2020) 100486.

[2] H. Dommati, S.S. Ray, J.C. Wang, S.S. Chen, A comprehensive review of recent developments in 3D printing technique for ceramic membrane fabrication for water purification, RSC Adv. 9 (2019) 16869–16883.

[3] S. Mazinani, A. Al-Shimmery, Y.M. John Chew, D. Mattia, 3D printed fouling-resistant composite

Membranes, ACS Appl. Mater. Interfaces. 11 (2019) 26373–26383.

[4] Z.X. Low, Y.T. Chua, B.M. Ray, D. Mattia, I.S. Metcalfe, D.A. Patterson, Perspective on 3D printing of separation membranes and comparison to related unconventional fabrication techniques, J. Memb. Sci. 523 (2017) 596–613.

[5] T. Femmer, A.J.C. Kuehne, M. Wessling, Print your own membrane: Direct rapid prototyping of polydimethylsiloxane, Lab Chip. 14 (2014) 2610–2613.

[6] S. Badalov, C.J. Arnusch, Ink-jet printing assisted fabrication of thin film composite membranes, J. Memb. Sci. 515 (2016) 79–85.

[7] N. Sreedhar, N. Thomas, O. Al-Ketan, R. Rowshan, H. H. Hernandez, R.K. Abu Al-Rub, H.A. Arafat, 3D printed feed spacers based on triply periodic minimal surfaces for flux enhancement and biofouling mitigation in RO and UF, Desalination. 425 (2018) 12–21.

[8] N. Sreedhar, N. Thomas, O. Al-Ketan, R. Rowshan, H.H. Hernandez, R.K. Abu Al-Rub, H.A. Arafat, Mass transfer analysis of ultrafiltration using spacers based on triply periodic minimal surfaces: Effects of spacer design, directionality and voidage, J. Memb. Sci. 561 (2018) 89–98.

[9] N. Thomas, N. Sreedhar, O. Al-Ketan, R. Rowshan, R.K. Abu Al-Rub, H.A. Arafat, 3D printed triply periodic minimal surfaces as spacers for enhanced heat and mass transfer in membrane distillation, Desalination. 443 (2018) 256–271.

[10] N. Thomas, N. Sreedhar, O. Al-Ketan, R. Rowshan, R.K. Abu Al-Rub, H. Arafat, 3D printed spacers based on TPMS architectures for scaling control in membrane distillation, J. Memb. Sci. 581 (2019) 38–49.

[11] E.H.C. Castillo, N. Thomas, O. Al-Ketan, R. Rowshan, R.K. Abu Al-Rub, L.D. Nghiem, S. Vigneswaran, H.A. Arafat, G. Naidu, 3D printed spacers for organic fouling mitigation in membrane distillation, J. Memb. Sci. 581 (2019) 331–343.

[12] C. Fritzmann, M. Wiese, T. Melin, M. Wessling, Helically microstructured spacers improve mass transfer and fractionation selectivity in ultrafiltration, J. Memb. Sci. 463 (2014) 41–48.

[13] A. Siddiqui, N. Farhat, S.S. Bucs, R.V. Linares, C. Picioreanu, J.C. Kruithof, M.C.M. Van Loosdrecht, J. Kidwell, J.S. Vrouwenvelder, Development and characterization of 3D-printed feed spacers for spiral wound membrane systems, Water Res. 91 (2016) 55–67.

[14] N. Yanar, M. Son, E. Yang, Y. Kim, H. Park, S. Nam, H. Choi, Investigation of the performance behavior of a forward osmosis membrane system using various feed spacer materials fabricated by 3D printing technique, Chemosphere. 202 (2018) 708–715.

[15] T. Luelf, D. Rall, D. Wypysek, M. Wiese, T. Femmer, C. Bremer, J.U. Michaelis, M. Wessling, 3D-printed rotating spinnerets create membranes with a twist, J. Memb. Sci. 555 (2018) 7–19.

[16] T. Femmer, F. Carstensen, M. Wessling, A membrane stirrer for product recovery and substrate feeding, Biotechnol. Bioeng. 112 (2015) 331–338.

[17] H.Y. Tsai, A. Huang, J.F. soesanto, Y.L. Luo, T.Y. Hsu, C.H. Chen, K.J. Hwang, C.D. Ho, K.L. Tung, 3D printing design of turbulence promoters in a cross-flow microfiltration system for fine particles removal, J. Memb. Sci. 573 (2019) 647–656.

[18] J.Y. Lee, W.S. Tan, J. An, C.K. Chua, C.Y. Tang, A.G. Fane, T.H. Chong, The potential to enhance membrane module design with 3D printing technology, J. Memb. Sci. 499 (2016) 480–490.

[19] J. Balster, I. Pünt, D.F. Stamatialis, M. Wessling, Multi-layer spacer geometries with improved mass transport, J. Memb. Sci. 282 (2006) 351–361.

[20] C. Fritzmann, M. Hausmann, M. Wiese, M. Wessling, T. Melin, Microstructured spacers for submerged membrane filtration systems, J. Memb. Sci. 446 (2013) 189–200.

[21] B. Wu, Y. Zhang, Z. Mao, W.S. Tan, Y.Z. Tan, J.W. Chew, T.H. Chong, A.G. Fane, Spacer vibration for fouling control of submerged flat sheet membranes, Sep. Purif. Technol. 210 (2019) 719–728.

[22] S. Kerdi, A. Qamar, J.S. Vrouwenvelder, N. Ghaffour, Fouling resilient perforated feed spacers for membrane filtration, Water Res. 140 (2018) 211–219.

[23] H.H. Salih, S.A. Dastgheib, Treatment of a hypersaline brine, extracted from a potential CO2 sequestration site, and an industrial wastewater by membrane distillation and forward osmosis, Chem. Eng. J. 325 (2017) 415–423.

[24] S. Leaper, A. Abdel-Karim, T.A. Gad-Allah, P. Gorgojo, Air-gap membrane distillation as a one-step process for textile wastewater treatment, Chem. Eng. J. 360 (2019) 1330–1340.

[25] J.-P. Mericq, S. Laborie, C. Cabassud, Evaluation of systems coupling vacuum membrane distillation and solar energy for seawater desalination, Chem. Eng. J. 166 (2011) 596–606.

[26] A. Ali, P. Aimar, E. Drioli, Effect of module design and flow patterns on performance of membrane distillation process, Chem. Eng. J. 277 (2015) 368–377.

[27] N. Thomas, M.O. Mavukkandy, S. Loutatidou, H.A. Arafat, Membrane distillation research & implementation: Lessons from the past five decades, Sep. Purif. Technol. 189 (2017) 108–127.

[28] J.A. Andrés-Mañas, A. Ruiz-Aguirre, F.G. Acién, G. Zaragoza, Performance increase of membrane distillation pilot scale modules operating in vacuum-enhanced air-gap configuration, Desalination. 475 (2020) 114202.

[29] A. Hagedorn, G. Fieg, D. Winter, J. Koschikowski, A. Grabowski, T. Mann, Membrane and spacer evaluation with respect to future module design in membrane distillation, Desalination. 413 (2017) 154–167.

[30] J. Seo, Y. Mi, J. Ha, Spacer optimization strategy for direct contact membrane distillation : Shapes,

configurations, diameters, and numbers of spacer filaments, Desalination. 417 (2017) 9–18.

[31] H.S. Abid, D.J. Johnson, R. Hashaikeh, N. Hilal, A review of efforts to reduce membrane fouling by control of feed spacer characteristics, Desalination. 420 (2017) 384–402.

[32] V. V. Ranade, A. Kumar, Fluid dynamics of spacer filled rectangular and curvilinear channels, J. Memb. Sci. 271 (2006) 1–15.

[33] M. Shakaib, S.M.F. Hasani, I. Ahmed, R.M. Yunus, A CFD study on the effect of spacer orientation on temperature polarization in membrane distillation modules, Desalination. 284 (2012) 332–340.

[34] J. Phattaranawik, R. Jiraratananon, A.G. Fane, Effects of net-type spacers on heat and mass transfer in direct contact membrane distillation and comparison with ultrafiltration studies, J. Memb. Sci. 217 (2003) 193–206.

[35] Y.D. Kim, L. Francis, J.G. Lee, M.G. Ham, N. Ghaffour, Effect of non-woven net spacer on a direct contact membrane distillation performance: Experimental and theoretical studies, J. Memb. Sci. 564 (2018) 193–203.

[36] S. Tielen, Enhancing reverse osmosis with feed spacer technology, Filtr. Sep. 53 (2016) 24–27.

[37] V.A. Haaksman, A. Siddiqui, C. Schellenberg, J. Kidwell, J.S. Vrouwenvelder, C. Picioreanu, Characterization of feed channel spacer performance using geometries obtained by X-ray computed tomography, J. Memb. Sci. 522 (2017) 124–139.

[38] W.S. Tan, S.R. Suwarno, J. An, C.K. Chua, A.G. Fane, T.H. Chong, Comparison of solid, liquid and powder forms of 3D printing techniques in membrane spacer fabrication, J. Memb. Sci. 537 (2017) 283–296.

[39] I. Campbell, O. Diegel, J. Kowen, T. Wohlers, Wohlers Report 2020: 3D Printing and additive manufacturing - Global state of the industry, 2020.

[40] D.G. Schniederjans, Y. Mehmet G, Perception of 3D-printing: analysis of manufacturing-use and adoption, Rapid Prototyp. J. 24 (2018) 510–520.

[41] J. Savolainen, M. Collan, How additive manufacturing technology changes business models? - Review of literature, Addit. Manuf. 32 (2020) 101070.

[42] O. Al-Ketan, R.K. Abu Al-Rub, Multifunctional mechanical metamaterials based on triply periodic minimal surface lattices, Adv. Eng. Mater. 21 (2019) 1–39.

[43] P. Yazgan-Birgi, M.I.H. Ali, J. Swaminathan, J.H. Lienhard, A. Arafat, Computational fluid dynamics modeling for performance assessment of permeate gap membrane distillation, J. Memb. Sci. 568 (2018) 55–66.

[44] I. Hitsov, K. De Sitter, C. Dotremont, I. Nopens, Economic modelling and model-based process optimization of membrane distillation, Desalination. 436 (2018) 125–143.

[45] K. DePalma, M.R. Walluk, A. Murtaugh, J. Hilton, S. McConky, B. Hilton, Assessment of 3D printing using fused deposition modeling and selective laser sintering for a circular economy, J. Clean. Prod. 264 (2020)

121567.

[46] S.R. Shah, N.C. Wright, P.A. Nepsky, A.G. Winter, Cost-optimal design of a batch electrodialysis system for domestic desalination of brackish groundwater, Desalination. 443 (2018) 198–211.

[47] D. Wirth, C. Cabassud, Membrane distillation for water desalination-optimisation of module design and operating conditions in regard with energy consumption, in: Eng. with Membr., Granada, 2001: p. 285.

[48] J. Xu, Y.B. Singh, G.L. Amy, N. Ghaffour, Effect of operating parameters and membrane characteristics on air gap membrane distillation performance for the treatment of highly saline water, J. Memb. Sci. 512 (2016) 73–82.

[49] F.A. Banat, J. Simandl, Desalination by Membrane Distillation : A Parametric Study, Sep. Purif. Technol. 33 (2008) 201–206.

[50] M.. García-Payo, M.. Izquierdo-Gil, C. Fernández-Pineda, Air gap membrane distillation of aqueous alcohol solutions, J. Memb. Sci. 169 (2000) 61–80.

[51] A.M. Alklaibi, N. Lior, Transport analysis of air-gap membrane distillation, J. Memb. Sci. 255 (2005) 239–253.

[52] A.M. Alklaibi, N. Lior, Comparative study of direct-contact and air-gap membrane distillation processes, Ind. Eng. Chem. Res. 46 (2007) 584–590.

[53] C.D. Ho, L. Chen, M.C. Huang, J.Y. Lai, Y.A. Chen, Distillate flux enhancement in the air gap membrane distillation with inserting carbon-fiber spacers, Sep. Sci. Technol. 52 (2017) 2815–2826.

[54] M.N. Chernyshov, G.W. Meindersma, A.B. de Haan, Comparison of spacers for temperature polarization reduction in air gap membrane distillation, Desalination. 183 (2005) 363–374.

[55] Y. Elhenawy, N.A.S. Elminshawy, M. Bassyouni, A. Alhathal Alanezi, E. Drioli, Experimental and theoretical investigation of a new air gap membrane distillation module with a corrugated feed channel, J. Memb. Sci. 594 (2020) 117461.

[56] A. Saeed, R. Vuthaluru, Y. Yang, H.B. Vuthaluru, Effect of feed spacer arrangement on flow dynamics through spacer filled membranes, Desalination. 285 (2012) 163–169.

[57] A.R. Da Costa, A.G. Fane, D.E. Wiley, Spacer characterization and pressure drop modeling in spacer-filled channels for ultrafiltration, J. Memb. Sci. 87 (1994) 79–98.

[58] Y. Taamneh, K. Bataineh, Improving the performance of direct contact membrane distillation utilizing spacer-filled channel, Desalination. 408 (2017) 25–35.

[59] J. Swaminathan, H.W. Chung, D.M. Warsinger, J.H. Lienhard V, Energy efficiency of membrane distillation up to high salinity: Evaluating critical system size and optimal membrane thickness, Appl. Energy. 211 (2018) 715–734.

[60] J. Swaminathan, H.W. Chung, D.M. Warsinger, J.H. Lienhard V, Membrane distillation model based on heat exchanger theory and configuration comparison, Appl. Energy. 184 (2016) 491–505.

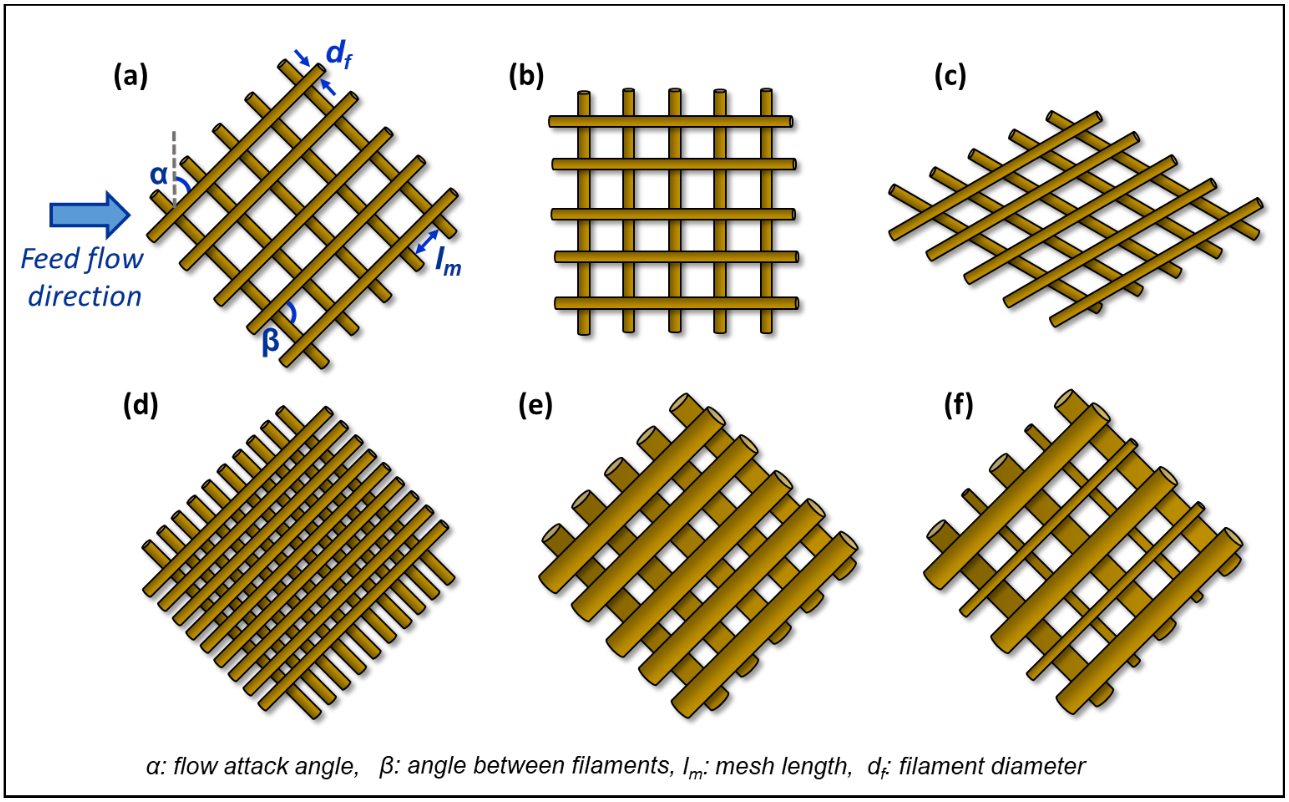

Fig. 1. (a) Geometric characteristics of non-woven mesh spacer and design variations obtained by altering the (b) flow attack angle, (c) angle between filaments, (d) mesh size, (e) filament thickness, and (f) alternating filament thickness.

(Artwork width - double column)

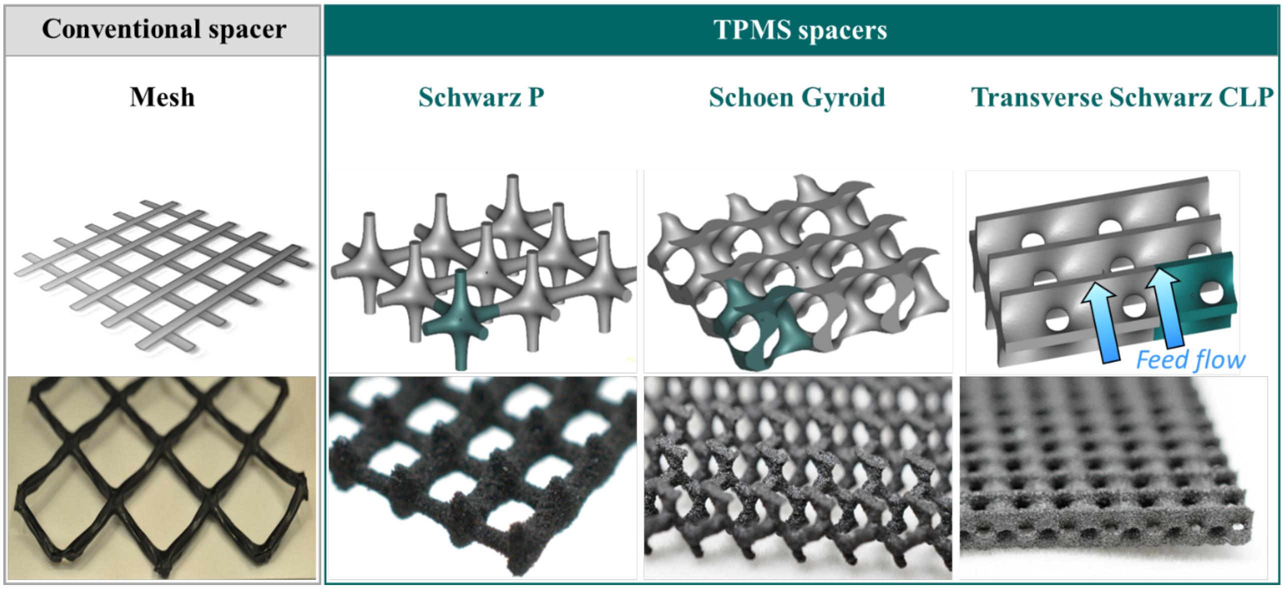

Fig. 2. Top row: depictions of the representative volume element of the spacers used in this study wherein for the TPMS spacers the green shaded region indicates a unit element. Bottom row: photographic images of the spacers.

(Artwork width - double column)

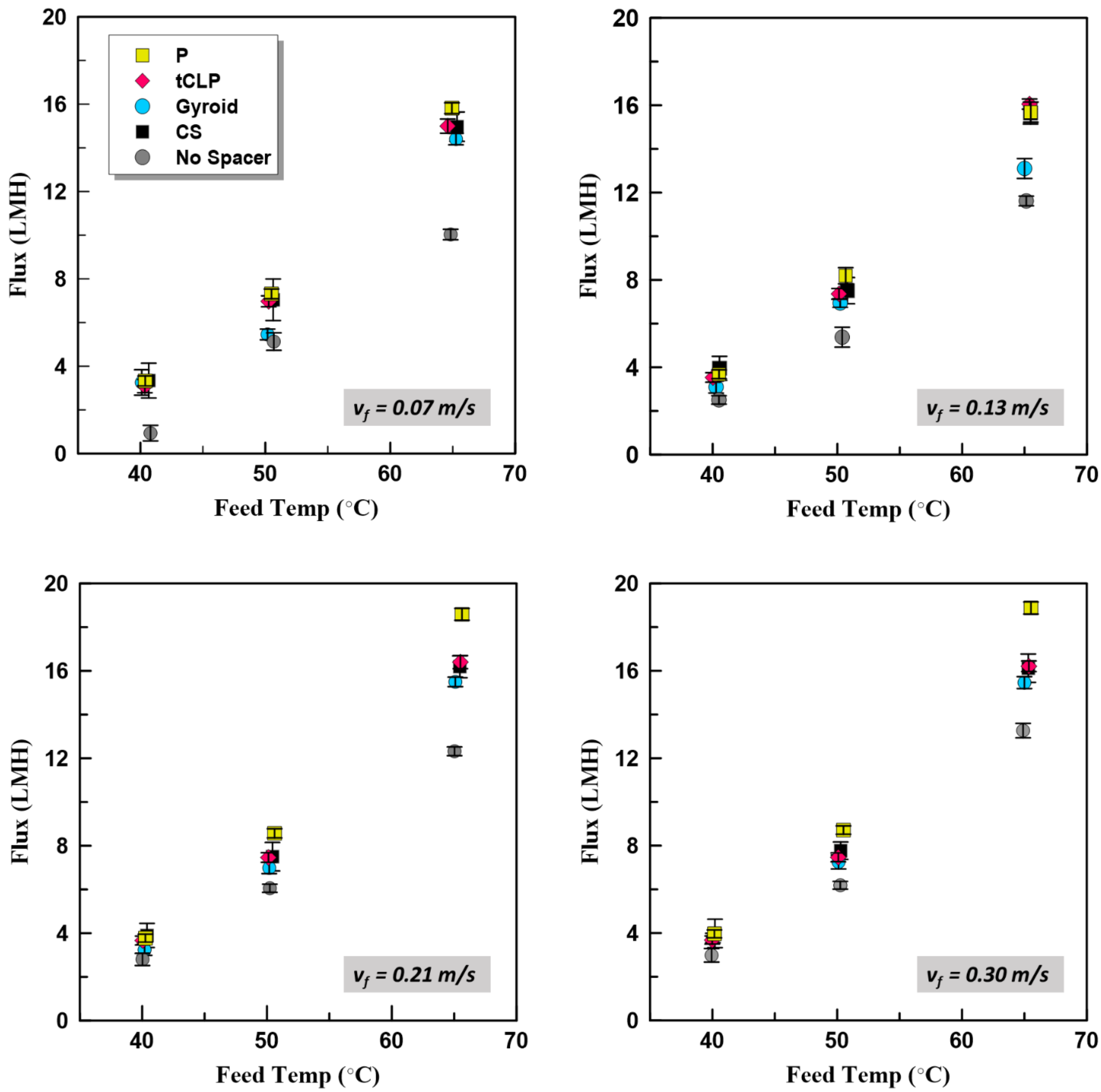

Fig. 3. AGMD flux performances of the TPMS spacers, commercial spacer (CS) and empty channel (no-spacer) condition at varying feed flow velocities and feed temperatures.

(Artwork width - double column)

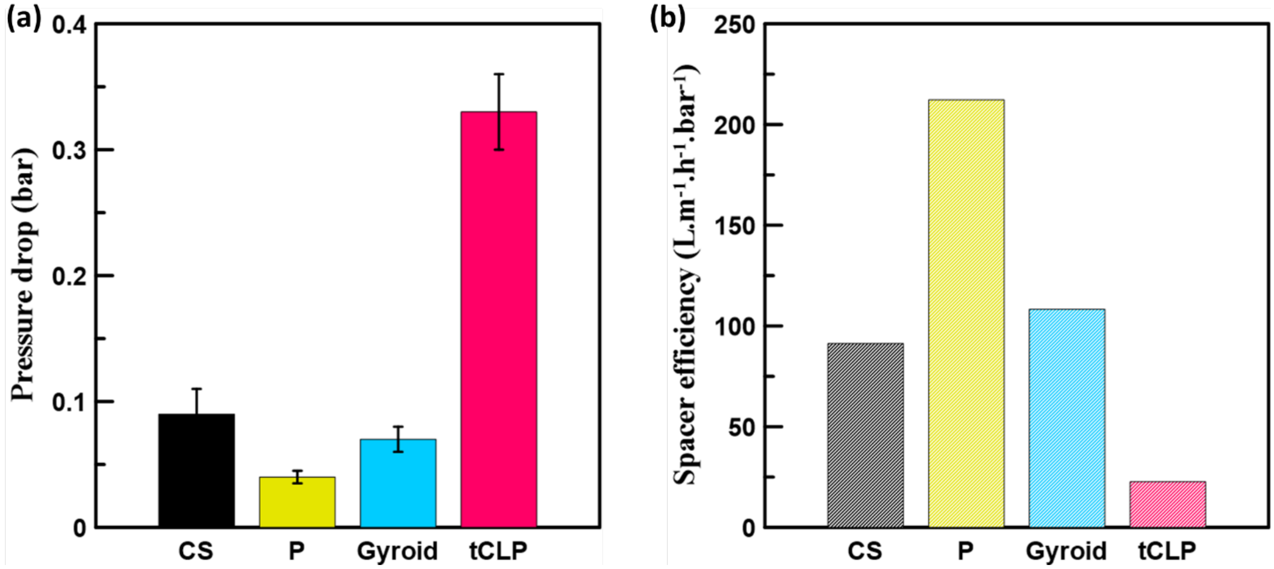

Fig. 4. Comparison of (a) pressure drop and (b) spacer efficiency with the use of CS and TPMS spacers in AGMD at a feed flow velocity of 0.30 m/s and feed temperature of 65 ºC.

(Artwork width - double column)

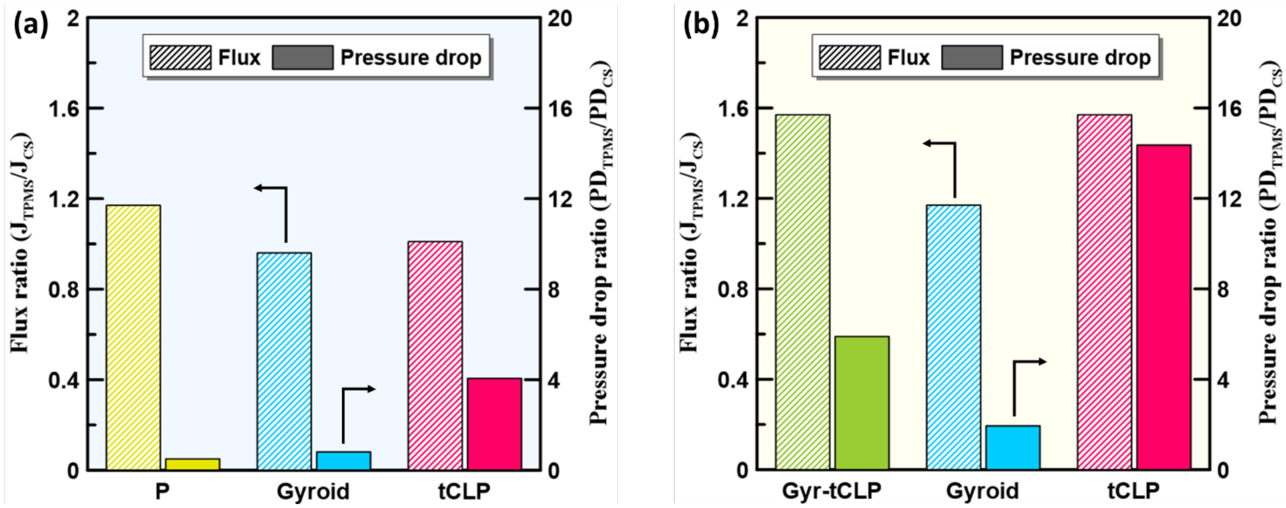

Fig. 5. Comparison of the relative flux and channel pressure drop ratio of three TPMS spacer geometries to a commercial spacer in (a) AGMD and (b) DCMD. The Gyr-tCLP spacer, tested in DCMD, combines the Gyr and tCLP geometry in a specific ratio [10].

(Artwork width - double column)

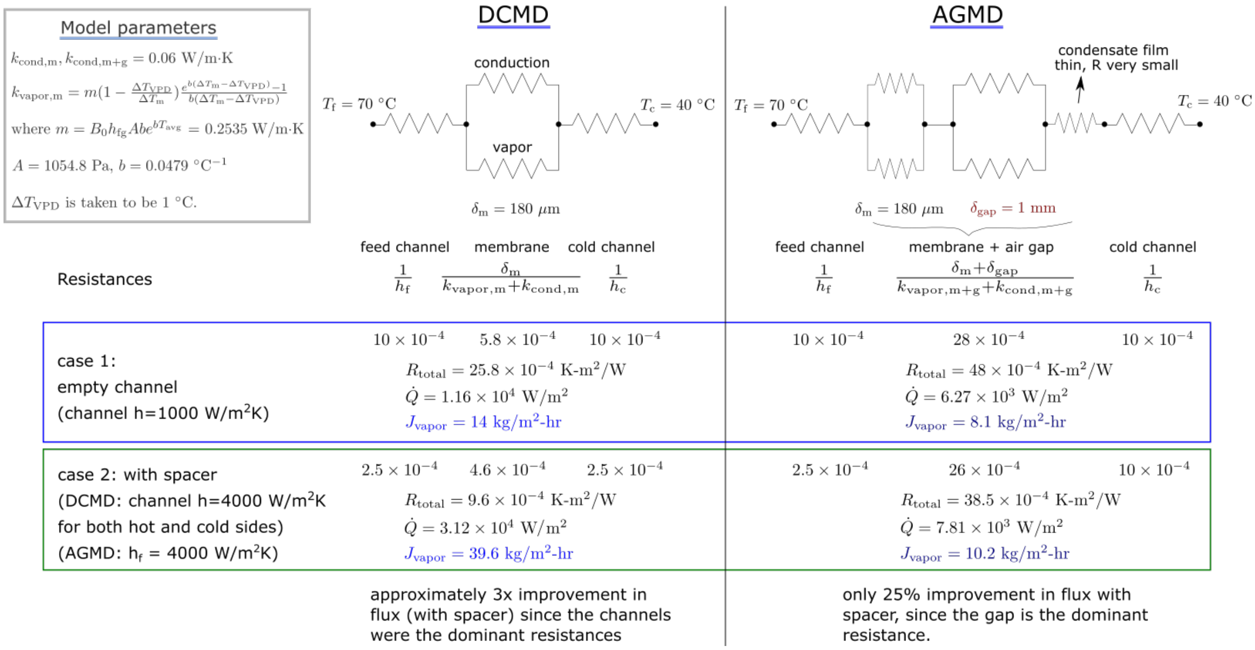

Fig. 6 Comparison of local water flux in DCMD and AGMD based on a simple resistance network model of both processes adapted from [59, 60]. Since the channel constitutes the major thermal resistance in DCMD, increasing the channel heat transfer coefficients by four-fold results in about 2.8 times higher flux. On the other hand, in AGMD, the gap constitutes the major thermal resistance. Therefore, increasing the heat transfer coefficient of the feed flow channel by four-fold, as in this study, results in an overall flux improvement of about 25% only.

(Artwork width - double column)

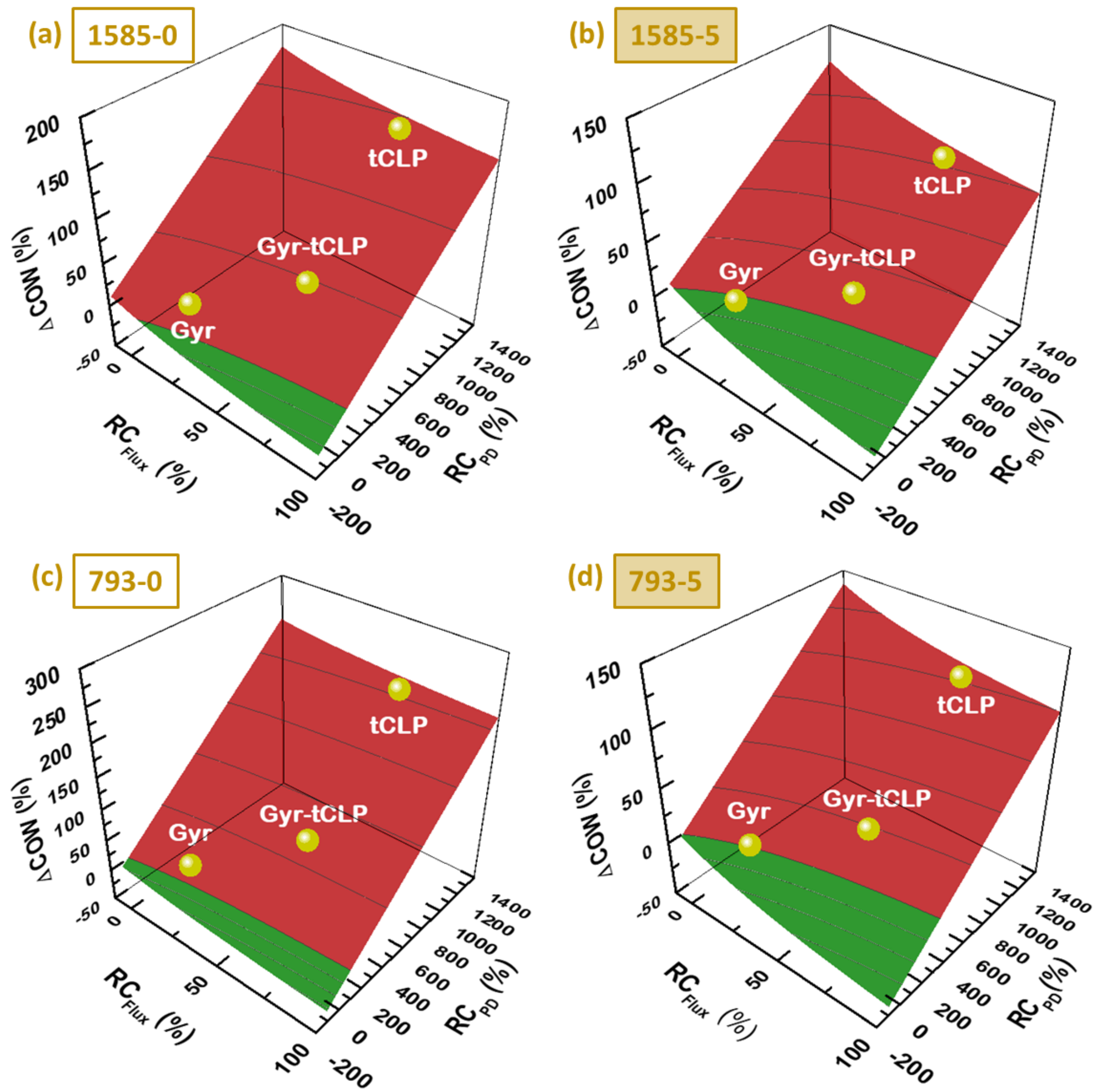

Fig. 7. Cost analysis for a small-scale (10 m^3/day) DCMD. Trends of the relative COW change when using TPMS spacers instead of CS are plotted for two different values of MD reference CAPEX (current: \$1585/m^2 and prospective: \$793/m^2) and two scenarios: free (waste) heat (left plots) and additional heat costs of \$5/m^3 (right plots). The green region of the curve is that of a favorable negative variation, or a relative decrease in COW. The red region shows a positive variation, or a relative increase in COW. Results for the TPMS spacers considered in this work are also shown on the curve.

(Artwork width - double column)

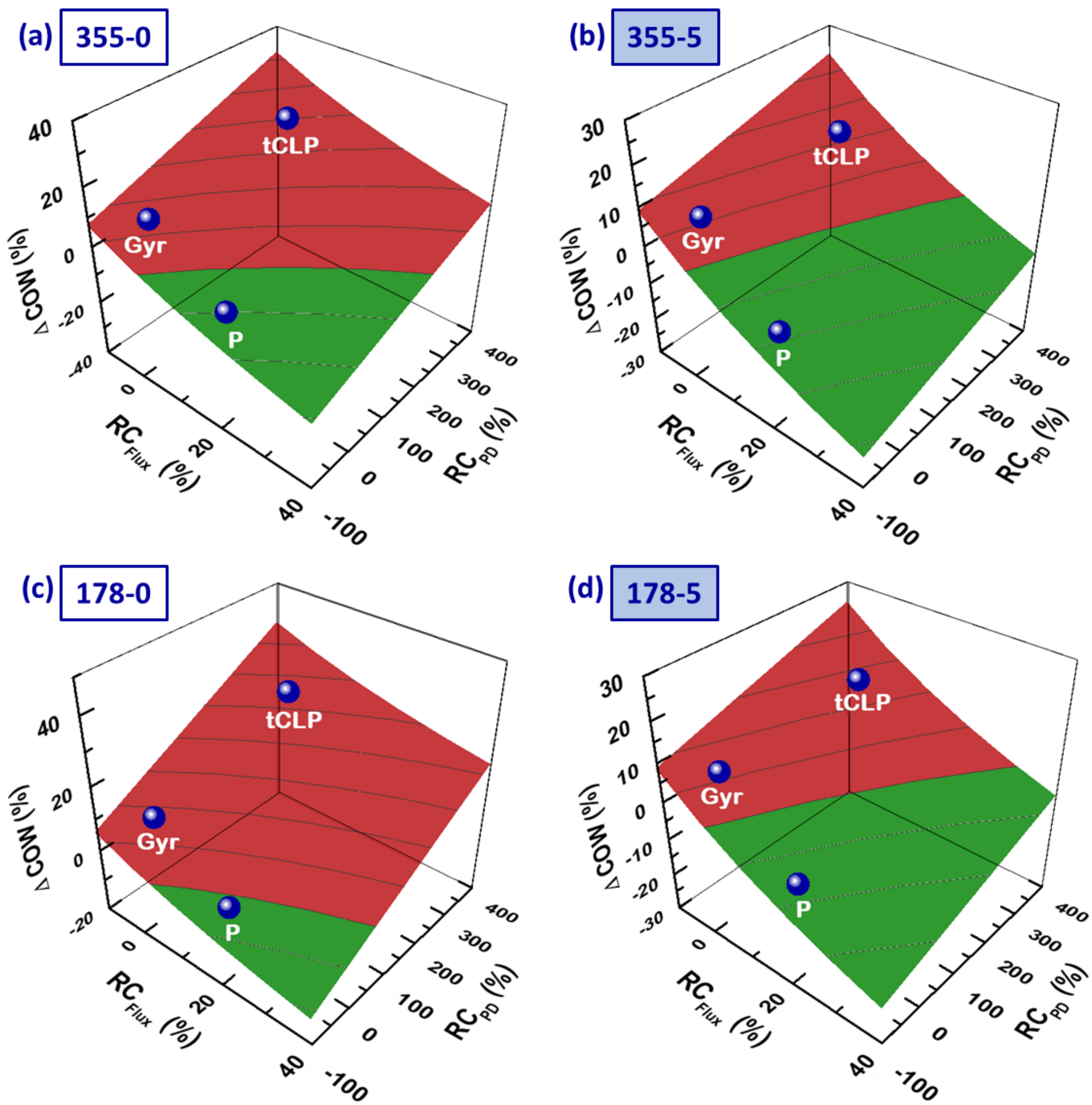

Fig. 8. Cost analysis for a small-scale (10 m^3/day) AGMD. Trends of the relative COW change when using TPMS spacers instead of CS are plotted for two different values of MD reference CAPEX (current: \$355/m^2 and prospective: \$178/m^2) and two scenarios: free (waste) heat (left plots) and additional heat costs of \$5/m^3 (right plots). The green region of the curve is that of a favorable negative variation, or a relative decrease in COW. The red region shows a positive variation, or a relative increase in COW. Results for the TPMS spacers considered in this work are also shown on the curve.

(Artwork width - double column)

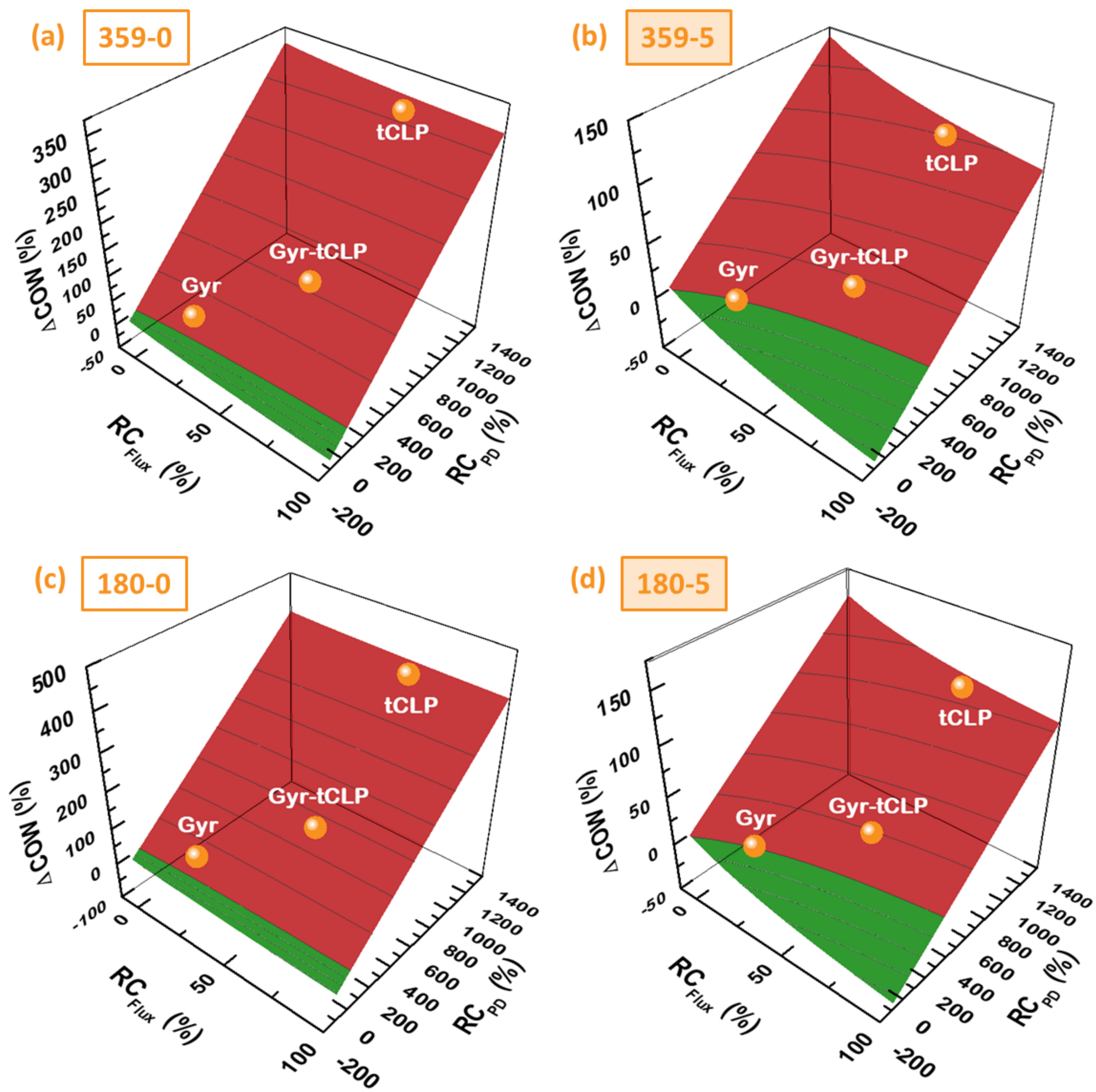

Fig. 9. Cost analysis for a large-scale (1000 m^3/day) DCMD. Trends of the relative COW change when using TPMS spacers instead of CS are plotted for two different values of MD reference CAPEX (current: \$359/m^2 and prospective: \$180/m^2) and two scenarios: free (waste) heat (left plots) and additional heat costs of \$5/m^3 (right plots). The green region of the curve is that of a favorable negative variation, or a relative decrease in COW. The red region shows a positive variation, or a relative increase in COW. Results for the TPMS spacers considered in this work are also shown on the curve.

(Artwork width - double column)

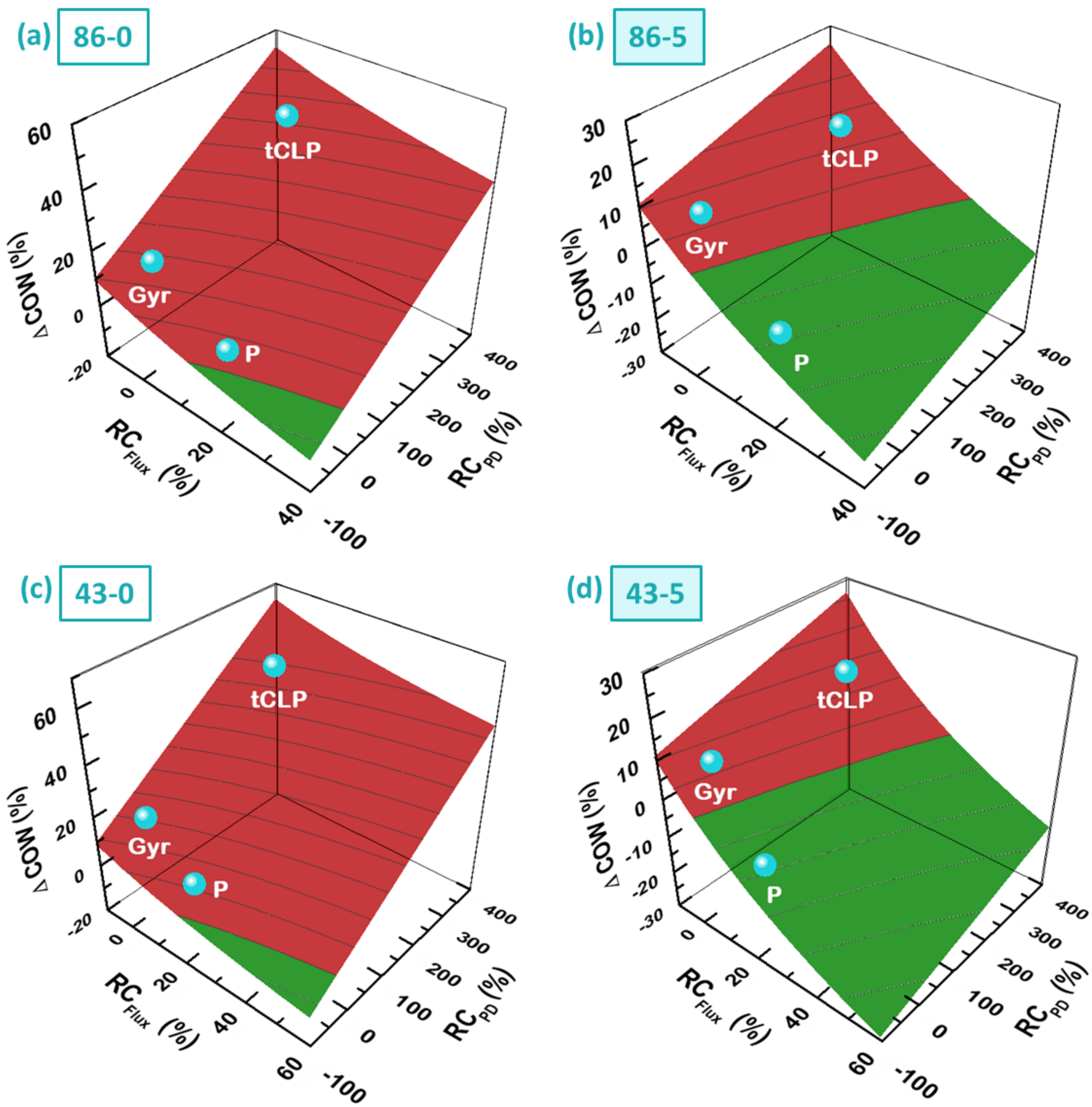

Fig. 10. Cost analysis for a large-scale (1000 m^3/day) AGMD. Trends of the relative COW change when using TPMS spacers instead of CS are plotted for two different values of MD reference CAPEX (current: \$86/m^2 and prospective: \$43/m^2) and two scenarios: free (waste) heat (left plots) and additional heat costs of \$5/m^3 (right plots). The green region of the curve is that of a favorable negative variation, or a relative decrease in COW. The red region shows a positive variation, or a relative increase in COW. Results for the TPMS spacers considered in this work are also shown on the curve.

(Artwork width - double column)

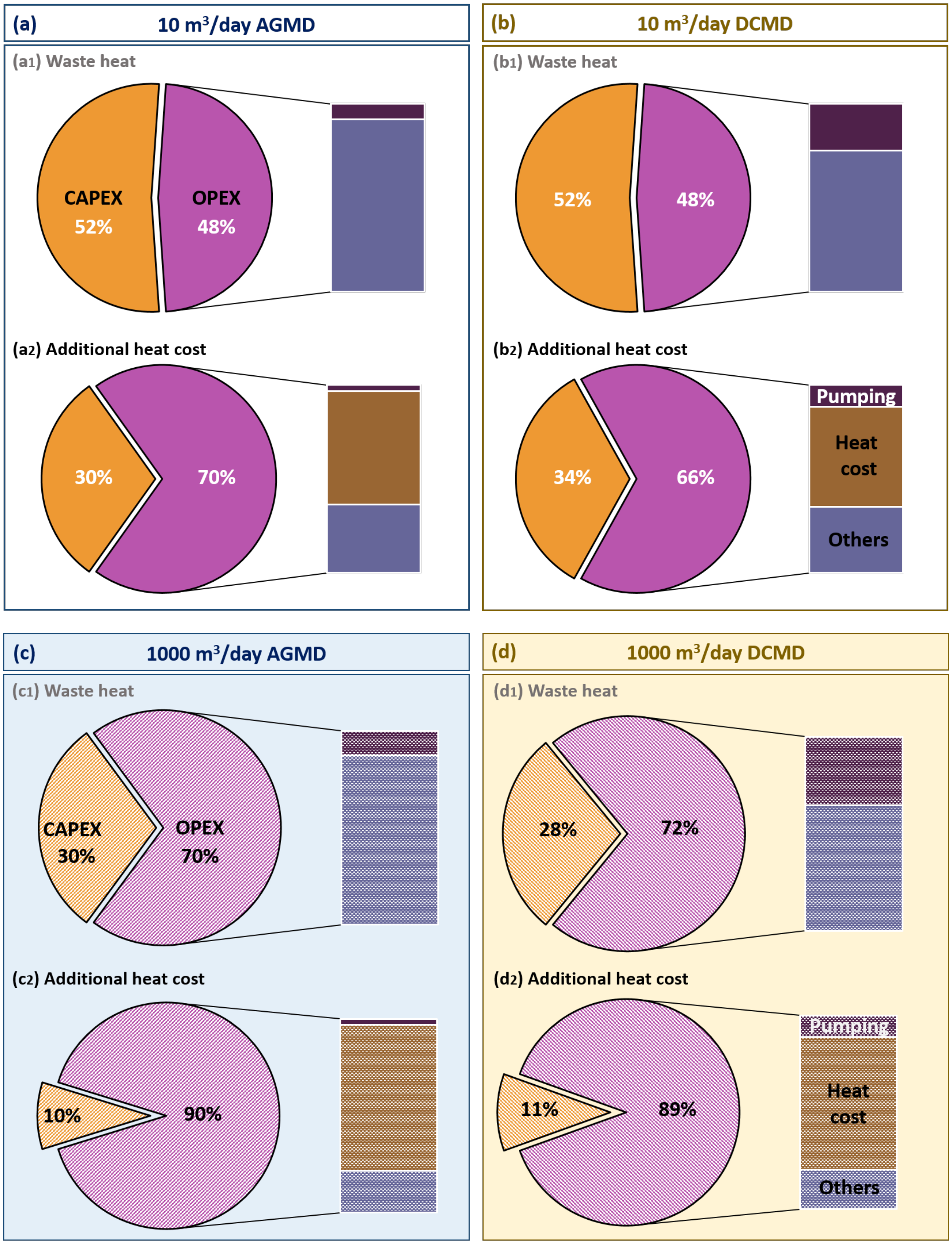

Fig. 11. Breakdown of COW for small and large-scale AGMD and DCMD plants based on current values of MD reference costs and using CS.

(Artwork width - double column)

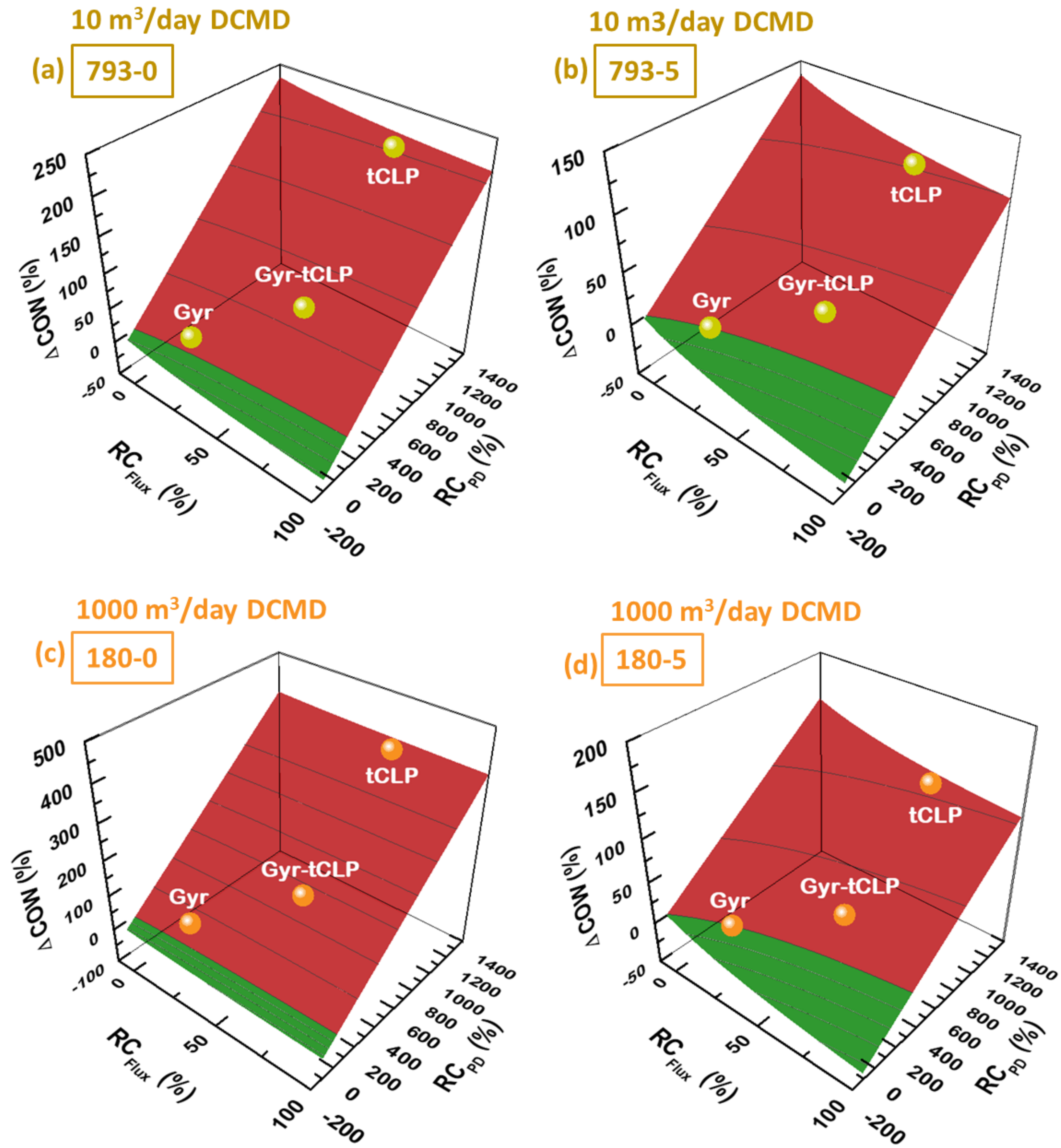

Fig. 12. Cost analysis for a small (10 m^3/day) and large-scale (1000 m^3/day) DCMD plant with the potential cost of 3D printed spacer as \$20/m^2. Trends of the relative COW change when using TPMS spacers instead of CS are plotted for values of prospective MD reference CAPEX with waste heat and additional heat cost.

(Artwork width - double column)

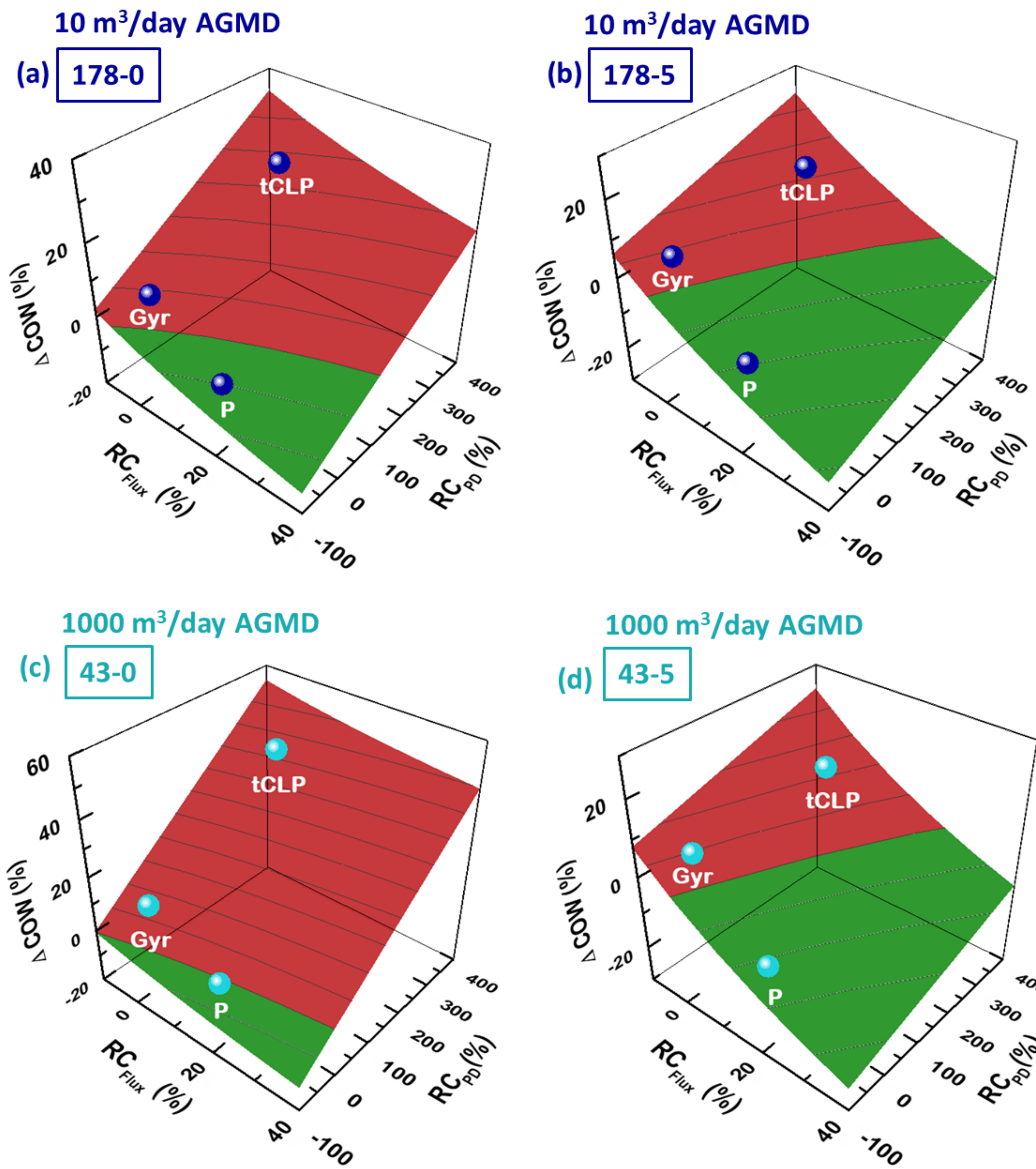

Fig. 13. Cost analysis for a small (10 m^3/day) and large-scale (1000 m^3/day) AGMD plant with the potential cost of 3D printed spacer as \$20/m^2. Trends of the relative COW change when using TPMS spacers instead of CS are plotted for values of prospective MD reference CAPEX with waste heat and additional heat cost.

(Artwork width - double column)

Table 1. Geometric characteristics of the TPMS spacers

TPMS design	Abbreviation	Porosity (%)	Surface area/Volume (mm^{-1})
Schwarz P	P	86	3.1
Schoen Gyroid	Gyr	84	4.1
Transverse Schwarz CLP	tCLP	88	7.9

Table 2. Properties of the AGMD module used in this study

Property	Value
Membrane module length	16 cm
Membrane module width	12 cm
Feed flow channel depth	4 mm
Active membrane area	192 cm^2
Air gap thickness	1 mm
Condensation plate material	Aluminum
Condensation plate thickness	4.8 mm
Coolant flow channel depth	10 mm

Table 3. Cost data for a small production scale MD plant (10 m^3/day) based on AGMD and DCMD configurations [45]

		AGMD	DCMD
Current			
$CAPEX_{CS}$	[$/$m^2$]	355	1585
COW_{CS_CAP}	[$/$m^3$]	3.60	4.80
$COW_{CS\text{-}OP}$	[$/$m^3$]	3.30	4.40
$COW_{CS\text{-}OP\_pump}$	[$/$m^3$]	0.33	1.10
$COW_{CS\text{-}OP\_rest}$	[$/$m^3$]	2.97	3.30
Prospective			
$CAPEX_{CS}^{*}$	[$/$m^2$]	178	793
$COW_{CS\text{-}CAP}^{*}$	[$/$m^3$]	1.80	2.40
$COW_{CS\text{-}OP}^{\dagger}$	[$/$m^3$]	3.30	4.40
$COW_{CS\text{-}OP\_pump}^{\dagger}$	[$/$m^3$]	0.33	1.10
$COW_{CS\text{-}OP\_rest}^{\dagger}$	[$/$m^3$]	2.97	3.30

*Based on personal communication with Mr. Bart Nelemans, Aquastill B.V., it is understood that the prospective capital cost for MD technology (once fully commercialized) will drop by up to 50%. This prospective reduction in MD module cost is herein reflected as a corresponding drop in CAPEX. Hence, prospective $COW_{CS\text{-}CAP}$ was also presented as 50% lower than the current $COW_{CS\text{-}CAP}$.

† For $COW_{CS\text{-}OP}$ and its sub-components, it is safe to assume that the drop in the MD module cost will not cause a drop in OPEX and hence same values as current costs are considered.

Table 4. Cost data for a large production scale MD plant (1000 m^3/day) based on AGMD and DCMD configurations [45]

		AGMD	DCMD
Current			
$CAPEX_{CS}$	[$/$m^2$]	86	359
$COW_{CS\text{-}CAP}$	[$/$m^3$]	0.70	0.90
$COW_{CS\text{-}OP}$	[$/$m^3$]	1.65	2.31
$COW_{CS\text{-}OP\_pump}$	[$/$m^3$]	0.22	0.77
$COW_{CS\text{-}OP\_rest}$	[$/$m^3$]	1.43	1.54
Prospective			
$CAPEX_{CS}{}^{*}$	[$/$m^2$]	43	180
$COW_{CS\text{-}CAP}{}^{*}$	[$/$m^3$]	0.35	0.45
$COW_{CS\text{-}OP}{}^{\dagger}$	[$/$m^3$]	1.65	2.31
$COW_{CS\text{-}OP\_pump}{}^{\dagger}$	[$/$m^3$]	0.22	0.77
$COW_{CS\text{-}OP\_rest}{}^{\dagger}$	[$/$m^3$]	1.43	1.54

* Based on personal communication with Mr. Bart Nelemans, Aquastill B.V., it is understood that the prospective capital cost for MD technology (once fully commercialized) will drop by up to 50%. This prospective reduction in MD module cost is herein reflected as a corresponding drop in CAPEX. Hence, prospective $COW_{CS\text{-}CAP}$ was also presented as 50% lower than the current $COW_{CS\text{-}CAP}$.

† For $COW_{CS\text{-}OP}$ and its sub-components, it is safe to assume that the drop in the MD module cost will not cause a drop in OPEX and hence same values as current costs are considered.

Table 5. Relative change in COW when using Gyroid (Gyr) TPMS spacer instead of CS in small- and large-scale DCMD plants. The scenarios highlighted in green indicate a favorable reduction in ΔCOW (%) while the scenarios highlighted in red indicate a rise in ΔCOW (%).

10 m^3/day DCMD plant			**1000 m^3/day DCMD plant**		
$CAPEX_{CS}$ ($/$m^2$)	$COW_{CS\text{-}OP\_th.energy}$ ($/$m^3$)	ΔCOW (%)	$CAPEX_{CS}$ ($/$m^2$)	$COW_{CS\text{-}OP\_th.energy}$ ($/$m^3$)	ΔCOW (%)
1585	0	6.1	359	0	24.0
1585	5	-1.1	359	5	0.7
793	0	13.3	180	0	30.2
793	5	0.7	180	5	1.5

Table 6. Relative change in COW when using P TPMS spacer instead of CS in small- and large-scale AGMD plants. The scenarios highlighted in green indicate a favorable reduction in ΔCOW (%) while the scenarios highlighted in red indicate a rise in ΔCOW (%).

10 m^3/day AGMD plant			**1000 m^3/day AGMD plant**		
$CAPEX_{CS}$ ($/$m^2$)	$COW_{CS\text{-}OP\_th.energy}$ ($/$m^3$)	ΔCOW (%)	$CAPEX_{CS}$ **($/$m^2$)**	$COW_{CS\text{-}OP\_th.energy}$ ($/$m^3$)	ΔCOW (%)
355	0	-5.1	86	0	2.8
355	5	-9.2	86	5	-9.2
178	0	-1.7	43	0	5.8
178	5	-8.2	43	5	-8.9

Graphical abstract